Supporting Information

Cysteamine-modified Pd sites in covalent organic framework for efficient electrocatalytic semi-hydrogenation of terminal alkynes

Shuai Liu,[a] Haoyan Zhang,[a] Pengxin Ren,[a] Jiangsheng Han,[b] Pengpeng Shao,[c] Yuyang Ge,[e] Guixian Chen,[a] Li Ma,*[a] Ling Wang,[a] Zhengfeng Zhao,[a] Baoying Li,[a] Siyuan Liu,[a] Yuehui Li,[f] Yongli Du,[a] Zunqi Liu,*[d] Jianbin Chen*[a,d]

[a]*School of Chemistry and Chemical Engineering, Qilu University of Technology (Shandong Academy of Sciences), Jinan 250353, China.*

[b]*School of Health&Nutrition, Wei Hai Vocationlal College, WeiHai 264200, China.*

[c]*College of Chemistry and Chemical Engineering, Hunan Key Laboratory of Micro & Nano Materials Interface Science, Central South University. 410083 Changsha, Hunan, P. R. China.*

[d]*Chemistry and Chemical Engineering College, Xinjiang Agricultural University, Urumqi 830052, China*

[e]*School of Chemistry and Chemical Engineering, Linyi University, Linyi 276000, China*

[f]*Smart College of Energy, Shanghai Jiao Tong University, No. 800 Dongchuan Road, Shanghai, 200240, China*

Email: li_ma@qlu.edu.cn; lzq@xjau.edu.cn; jchen@qlu.edu.cn

Table of Contents

Section 1. General Information

Chemicals and materials

1,3,5-triformylphloroglucinol (Tp, 99.3%) and 5,5′-diamino-2,2′-bipyridine (Bpy, 99%) were purchased from Jilin Chinese Academy of Sciences-Yanshen Technology Co., Ltd. *N*,*N*-Dimethylacetamide (DMAc, 99%) and 1,2-dichlorobenzene (*o*-DCB) were purchased from Energy Chemical. Acetic acid (CH_3COOH, AR) was purchased from Fuyu Chemical. Palladium(II) acetate ($Pd(OCOCH_3)_2$, 98%) was purchased from Leyan. Cysteamine (C_2H_7NS, 98%) was purchased from Shanghai Macklin Biochemical Technology Co., Ltd.

Characterizations

Sample morphology was observed using a SEM5000X field-emission scanning electron microscope from CIQTE Co., Ltd. Transmission electron microscopy (TEM) images were acquired on a JEOL JEM-2100F instrument. Surface chemical states were characterized by X-ray photoelectron spectroscopy (XPS) on a Thermo Scientific K-Alpha spectrometer, with XPS data calibrated to the adventitious carbon C 1s peak at 284.8 eV. Pd concentrations were determined by inductively coupled plasma-optical emission spectrometry (ICP-OES) using an Agilent 5110 instrument. Powder X-ray diffraction (PXRD) patterns were collected on a Rigaku SmartLab SE diffractometer over a 2θ range of 3° to 60° at a scan rate of 20° min^{-1}. Electron paramagnetic resonance (EPR) spectra were recorded at 100 K and 9.5 GHz on a Bruker EMXplus spectrometer. Fourier-transform infrared (FTIR) spectra were obtained using a Thermo iS50 spectrometer. Brunauer-Emmett-Teller (BET) specific surface areas and pore size distributions were measured with an Autosorb-iQ-MP analyzer. Nuclear magnetic resonance (NMR) spectra (^1H NMR: 400 MHz; ^{13}C NMR: 101 MHz) were recorded on a JEOL JNM-ECZL400S instrument using $CDCl_3$ as solvent; chemical shifts are reported in ppm relative to tetramethylsilane with peak multiplicities denoted as s (singlet), d (doublet), t (triplet), m (multiplet), and br (broad), and coupling constants (J) reported in Hz. Quantitative analysis of products was performed by high-performance liquid chromatography (HPLC) on a Shimadzu Prominence Plus LC-20A system using an isocratic elution with mobile phase A (acetonitrile) and B (5% acetic acid aqueous solution) at a ratio of 7:3 for 22

min at a flow rate of 1 mL/min. Identification of reactants and products was carried out by gas chromatography-mass spectrometry (GC-MS) on a Shimadzu GCMS-TQ8040 system equipped with an Rtx-5MS capillary column (0.25 mm in diameter, 30 m in length).

Section 2. Experimental Section

Preparation of TpBpy COF

A Schlenk tube was charged with Tp (105 mg, 0.5 mmol) and Bpy (140 mg, 0.75 mmol). N,N-Dimethylacetamide (7.5 mL) and 1,2-dichlorobenzene (2.5 mL) were added as solvents, followed by the addition of 6 M AcOH (1 mL) via micropipette. Ultrasonication was performed on the mixture (15 min) to ensure complete dispersion. After sonication, the mixture was rapidly frozen in a liquid nitrogen bath and subjected to three freeze-pump-thaw cycles for degassing before vacuum sealing. A 72 h heating process at 120 °C was applied to the sealed tube. Upon completion, the resulting dark red precipitate was collected via filtration, washed sequentially with DMAc, water, and acetone (5-6 times each) to remove unreacted monomers. TpBpy COF was obtained as a dark red powder after vacuum drying.

Synthesis of Pd-TpBpy COF

Palladium (II) acetate (56 mg) was placed in a round-bottom flask, followed by the addition of dichloromethane (DCM, 28 mL). After sonication, a uniform solution was obtained. Subsequently, TpBpy COF powder (50 mg) was dispersed into this solution. After stirring at room temperature for 6 h, the solid product was filtered and Soxhlet-extracted with DCM for 8 h. Finally, the solid product was vacuum-dried at 60 °C overnight to afford Pd-TpBpy COF.

Preparation of Pd-TpBpy/Cys COF

Cysteamine (193 mg) was dissolved in a mixture consisting of anhydrous ethanol (8 mL) and water (2 mL). Pd-TpBpy COF (50 mg) was then dispersed in the resulting solution. After stirring the mixture at 30 °C for 6 h, the solid product was then filtered, washed (water → anhydrous

ethanol), and vacuum-dried at 60 °C overnight to give Pd-TpBpy/Cys COF catalyst.

Synthesis of Pd-TpBpy/Pro COF and Pd-TpBpy/Dod COF

The synthetic procedures for Pd-TpBpy/Pro COF and Pd-TpBpy/Dod COF were analogous to that of Pd-TpBpy/Cys COF, except that cysteamine (193 mg) was substituted with propanethiol (225 μL) and dodecanethiol (598 μL), respectively, while maintaining all other reaction conditions.

Preparation of the working electrode

The carbon paper with a size of 1 × 2 cm^2 was pretreated in a 35% nitric acid solution (90 °C, 16 h), followed by rinsing with deionized water until neutral. Catalyst (10 mg), PVDF (1 mg), and XC-72R (carbon black, 1 mg) were ultrasonically dispersed in 1 mL of N-methylpyrrolidone. Subsequently, 500 μL of the above solution was deposited on each side of the carbon paper, forming a 1 × 1 cm^2 coating area. The catalyst loading was 5 mg/cm^2.

Electrochemical measurement

Electrochemical measurements were conducted using a CHI 760E electrochemical workstation in a standard three-electrode system. The electrolyte employed was 1 M KOH solution with 1,4-dioxane as a co-solvent. A Hg/HgO electrode (immersed in 3 M KCl) and a Pt foil (1 × 1 cm^2) served as the reference and counter electrodes, respectively. The working electrode was carbon paper loaded with catalyst (the catalyst loading was 5 mg/cm^2). All linear sweep voltammetry (LSV) tests, except those performed in a flow cell, were carried out in an H-type electrolytic cell separated by a Nafion 117 proton exchange membrane, with a scan rate of 10 mV s^{-1}. To evaluate the electrochemical active surface area (ECSA) of the as-prepared catalysts, the electrochemical double-layer capacitance (Cdl) was determined via cyclic voltammetry (CV) at scan rates of 20, 40, 60, 80, and 100 mV s^{-1}. Furthermore, all electrochemical tests were performed without iR compensation.

General procedure of electrochemical semihydrogenation of alkynes

The electrocatalytic reaction was conducted in an H-type electrochemical cell equipped a Nafion 117 proton exchange membrane. Both chambers were charged with 1.0 M KOH aqueous solution (5 mL) and 1,4-dioxane (5 mL). LSV and chronoamperometry were performed using a CHI760E electrochemical workstation. For standard operation, 0.1 mmol alkyne was added to the cathode chamber and sonicated to afford a uniform solution, followed by chronoamperometry under stirring conditions. Upon reaction completion, the cathodic products were extracted with DCM. After removal of organic phase, the residual material was either purified by silica gel chromatography to determine isolated yields or analyzed by high-performance liquid chromatography (HPLC) to calculate HPLC yields. The aryl alkynes conversion was calculated according to standard calibration curves.

Calculations

The conversion of substrate was calculated using equation (1):

$$Conversion(\%) = \frac{mol\ of\ formed\ alkene}{mol\ of\ initial\ alkyne} \times 100\% \quad (1)$$

The selectivity of the product was calculated using equation (2):

$$Selectivity(\%) = \frac{mol\ of\ formed\ alkene}{mol\ of\ consumed\ alkyne} \times 100\% \quad (2)$$

The TOF and TON were calculated as shown in (3) and (4):

$$TON = \frac{mol\ of\ formed\ alkene}{mol\ of\ Pd} \quad (3)$$

$$TOF = \frac{TON}{Time} \quad (4)$$

Trapping the H radical by the EPR experiment

In the standard procedure for electrochemical semi-hydrogenation of alkynes, chronoamperometry was first performed at an applied potential of -1.1 V (vs. Hg/HgO) for 30 min, followed by the addition of the radical trapping agent DMPO (5,5-dimethyl-1-pyrroline N-oxide). After stirring for 2 minutes, the reaction solution proximal to the working electrode was then immediately sampled and transferred to an EPR tube within approximately 40 seconds for

spectroscopic analysis.

The capture of active *H with tertiary butanol (*t*-BuOH)

To ensure the reliability of comparative experiments, the Pd-TpBpy/Cys COF electrode was equally divided into two samples with equal areas, which were respectively used for the electrocatalytic semi-hydrogenation system of alkynes containing 50 μL *t*-BuOH and the system without *t*-BuOH. 0.1 mmol of substrate **1a** (4-ethynylbiphenyl) was added to the electrolytic cell for semi-hydrogenation reaction, and a chronoamperometric test was conducted at a constant potential of -1.1 V (vs. Hg/HgO) for 12 hours. The content of product **2a** was detected every 2 hours during the test.

Section 3. Supporting Figures and Tables

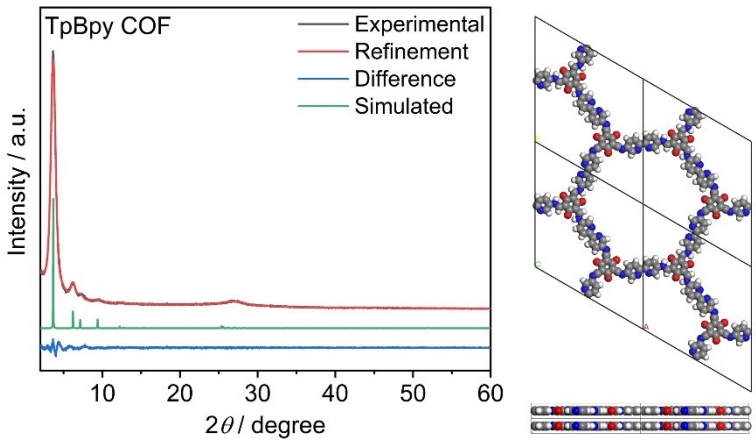

Fig. S1. The experimental PXRD pattern and its simulations of TpBpy COF. Experimentally PXRD pattern (gray), Pawley refinement (red), their difference (blue), simulated XRD pattern based on the eclipsed (green) stacking mode for corresponding TpBpy COF.

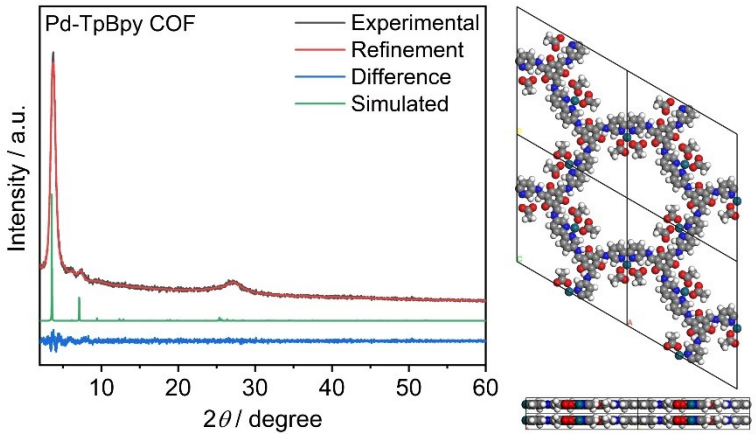

Fig. S2. The experimental PXRD pattern and its simulations of Pd-TpBpy COF. Experimentally PXRD pattern (gray), Pawley refinement (red), their difference (blue), simulated XRD pattern based on the eclipsed (green) stacking mode for corresponding Pd-TpBpy COF.

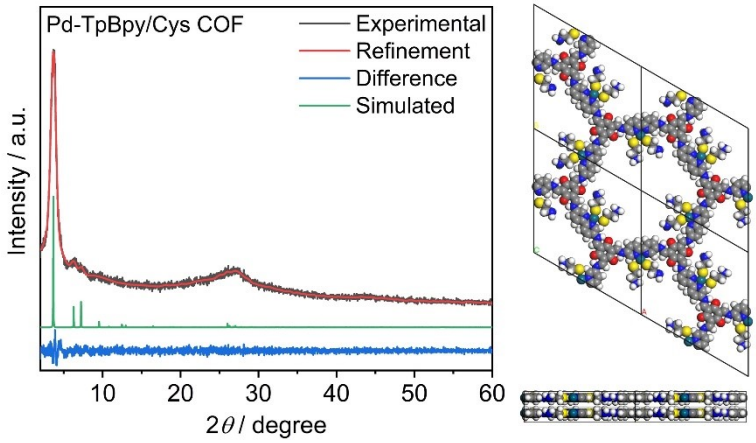

Fig. S3. The experimental PXRD pattern and its simulations of Pd-TpBpy/Cys COF. Experimentally PXRD pattern (gray), Pawley refinement (red), their difference (blue), simulated XRD pattern based on the eclipsed (green) stacking mode for corresponding Pd-TpBpy/Cys COF.

Table S1. Atomistic coordinates for the unit cell of TpBpy COF. Atomistic coordinates for the eclipsed mode of TpBpy COF optimized by using Materials Studio (space group P6, a = 29.3708 Å, b = 29.3708 Å, c = 3.5403 Å, α = 90°, β = 90°, γ = 120°, R_p = 3.94%, and R_{wp} = 5.51%).

Element	Atom number	x	y	z
C	C1	0.41441	0.51264	-0.5
C	C2	0.4466	0.48971	-0.5
C	C3	0.50213	0.52189	-0.5
N	N4	0.52162	0.5749	-0.5
C	C5	0.49194	0.59843	-0.5
C	C6	0.43648	0.56766	-0.5
C	C7	0.53818	0.50303	-0.5
C	C8	0.52397	0.44922	-0.5
N	N9	0.5907	0.5388	-0.5
C	C10	0.37218	0.65043	-0.5
C	C11	0.38699	0.70447	-0.5
O	O12	0.3024	0.56472	-0.5
C	C13	0.22426	0.5879	-0.5
N	N14	0.4139	0.81626	-0.5
C	C15	0.6294	0.52637	-0.5
C	C16	0.56304	0.43478	-0.5
C	C17	0.61685	0.47343	-0.5
C	C18	0.66145	0.37882	-0.5
C	C19	0.61634	0.32819	-0.5
O	O20	0.75208	0.42847	-0.5
C	C21	0.76384	0.34243	-0.5

Element	Atom number	x	y	z
N	N22	0.53598	0.19345	-0.5
H	H23	0.37441	0.48873	0.5
H	H24	0.42875	0.44971	0.5
H	H25	0.51072	0.63844	0.5
H	H26	0.48563	0.41991	0.5
H	H27	0.21543	0.54948	0.5
H	H28	0.44009	0.80527	0.5
H	H29	0.66773	0.55593	0.5
H	H30	0.55187	0.39588	0.5

Table S2. Atomistic coordinates for the unit cell of Pd-TpBpy COF. Atomistic coordinates for the eclipsed mode of Pd-TpBpy COF optimized by using Materials Studio (space group P3, a = 28.6419 Å, b = 28.6419 Å, c = 3.5124 Å, α = 90°, β = 90°, γ = 120°, R_p = 5.02%, and R_{wp} = 6.64%).

Element	Atom number	x	y	z
Pd	Pd1	0.52586	0.52563	0.57439
C	C2	0.33243	0.44441	0.57439
C	C3	0.35766	0.41376	0.57439
C	C4	0.41417	0.44026	0.57439
N	N5	0.44426	0.4952	0.57439
C	C6	0.42004	0.52453	0.57439
C	C7	0.36351	0.50063	0.57439
C	C8	0.44494	0.41261	0.57439
C	C9	0.42313	0.3561	0.57439
N	N10	0.49901	0.44609	0.57439
C	C11	0.34988	0.62516	0.57439
C	C12	0.39093	0.68343	0.57439
O	O13	0.25842	0.56147	0.57439
C	C14	0.2221	0.63192	0.57439
N	N15	0.46778	0.8051	0.57439
C	C16	0.53294	0.42679	0.57439
C	C17	0.4585	0.33568	0.57439
C	C18	0.51364	0.37241	0.57439
C	C19	0.61099	0.32412	0.57439
C	C20	0.61974	0.27828	0.57439
O	O21	0.65307	0.41994	0.57439
C	C22	0.75406	0.43982	0.57439
N	N23	0.64013	0.19481	0.57439
H	H24	0.28654	0.4237	0.57439
H	H25	0.33249	0.36787	0.57439
H	H26	0.44517	0.57042	0.57439

Element	Atom number	x	y	z
H	H27	0.37757	0.32812	0.57439
H	H28	0.19235	0.58671	0.57439
H	H29	0.48803	0.78067	0.57439
H	H30	0.57834	0.45573	0.57439
H	H31	0.44187	0.29026	0.57439
O	O32	0.50426	0.64826	0.57439
H	H33	0.60497	0.7249	0.27171
H	H34	0.63333	0.70697	0.68673
H	H35	0.58824	0.73549	0.76472
O	O36	0.55522	0.60624	0.57439
C	C37	0.54823	0.65199	0.57439
C	C38	0.59668	0.70831	0.57439
O	O39	0.65122	0.63267	0.57439
H	H40	0.72022	0.59777	0.27383
H	H41	0.69552	0.5487	0.67489
H	H42	0.73263	0.62242	0.77445
O	O43	0.60189	0.54051	0.57439
C	C44	0.65037	0.58994	0.57439
C	C45	0.70289	0.58969	0.57439
H	H46	0.74564	0.47474	0.57439
H	H47	0.60737	0.20483	0.57439

Table S3. Atomistic coordinates for the unit cell of Pd-TpBpy/Cys COF. Atomistic coordinates for the eclipsed mode of Pd-TpBpy/Cys optimized by using Materials Studio (space group P3, a = 28.6419 Å, b = 28.6419 Å, c = 3.4349 Å, α = 90°, β = 90°, γ = 120°, R_p = 5.39%, and R_{wp} = 7.05%).

Element	Atom number	x	y	z
Pd	Pd1	0.55971	0.55507	0.58734
C	C2	0.37004	0.48238	0.58734
C	C3	0.39787	0.45933	0.58734
C	C4	0.4541	0.48455	0.58734
N	N5	0.48055	0.53017	0.58734
C	C6	0.45337	0.55144	0.58734
C	C7	0.39794	0.52951	0.58734
C	C8	0.48784	0.46387	0.58734
C	C9	0.4676	0.41666	0.58734
N	N10	0.54149	0.4929	0.58734
C	C11	0.3638	0.6372	0.58734
C	C12	0.39248	0.6967	0.58734
O	O13	0.28056	0.56019	0.58734
C	C14	0.21956	0.60696	0.58734

Element	Atom number	x	y	z
N	N15	0.44469	0.81481	0.58734
C	C16	0.57664	0.47759	0.58734
C	C17	0.50293	0.40004	0.58734
C	C18	0.55794	0.43058	0.58734
C	C19	0.62422	0.34867	0.58734
C	C20	0.60959	0.2915	0.58734
O	O21	0.69444	0.43607	0.58734
C	C22	0.77576	0.41513	0.58734
N	N23	0.58564	0.18076	0.58734
N	N24	0.59524	0.75785	0.58734
S	S25	0.57464	0.62658	0.58734
C	C26	0.56098	0.67002	0.58734
C	C27	0.61103	0.72253	0.58734
N	N28	0.77422	0.72285	0.58734
S	S29	0.65163	0.57869	0.58734
C	C30	0.68658	0.64758	0.58734
C	C31	0.74579	0.66634	0.58734
H	H32	0.32415	0.45728	0.58734
H	H33	0.37708	0.41344	0.58734
H	H34	0.47349	0.59728	0.58734
H	H35	0.4218	0.39049	0.58734
H	H36	0.19858	0.56106	0.58734
H	H37	0.46789	0.79328	0.58734
H	H38	0.62146	0.50881	0.58734
H	H39	0.48853	0.35504	0.58734
H	H40	0.786	0.45905	0.58734
H	H41	0.55525	0.19401	0.58734
H	H42	0.58155	0.7608	0.29073
H	H43	0.62925	0.79773	0.67533
H	H44	0.53644	0.66642	0.85851
H	H45	0.53638	0.66634	0.31635
H	H46	0.6355	0.72704	0.3139
H	H47	0.63557	0.72606	0.85832
H	H48	0.8122	0.73763	0.75457
H	H49	0.74915	0.7379	0.72428
H	H50	0.67592	0.6632	0.85883
H	H51	0.67569	0.66309	0.31635
H	H52	0.75649	0.6508	0.3157
H	H53	0.75629	0.6505	0.85832

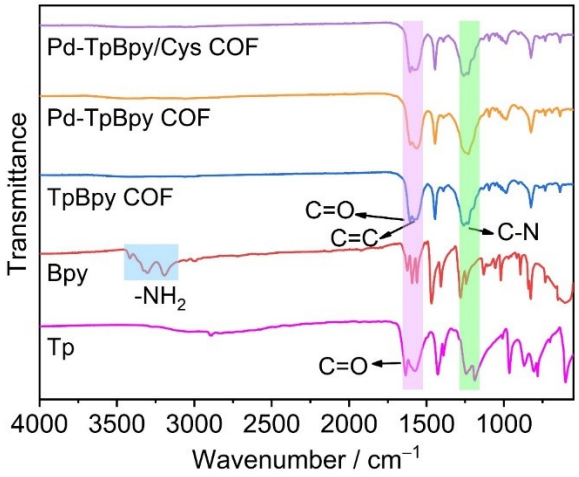

Fig. S4. FT-IR spectra of Tp, Bpy, TpBpy COF, Pd-TpBpy COF, and Pd-TpBpy/Cys COF.

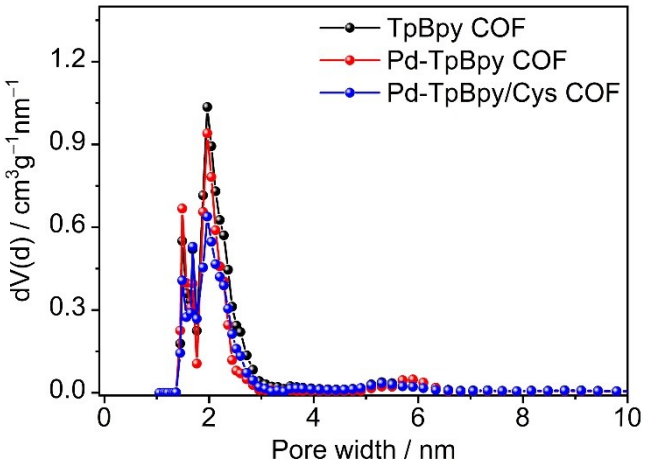

Fig. S5. Pore Size distribution analyses of TpBpy COF, Pd-TpBpy COF, and Pd-TpBpy/Cys COF, calculated based on the non-local density functional theory (cylindr.pores, NLDFT equilibrium model).

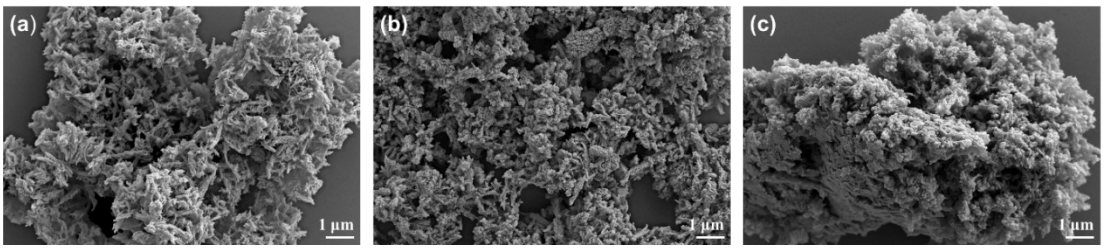

Fig. S6. SEM images of (a) TpBpy COF, (b) Pd-TpBpy COF, and (c)Pd-TpBpy/Cys COF.

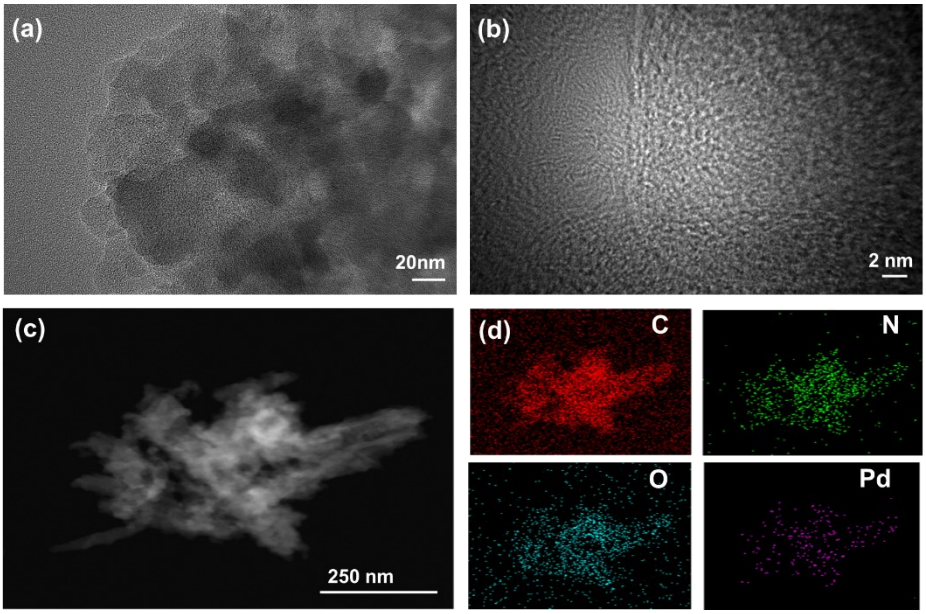

Fig. S7. (a, b) TEM images of Pd-TpBpy COF and (c, d) EDX mapping images of Pd-TpBpy COF.

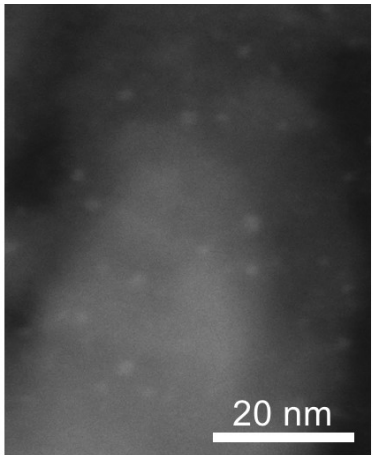

Fig. S8. HAADF-STEM image of Pd-TpBpy/Cys COF.

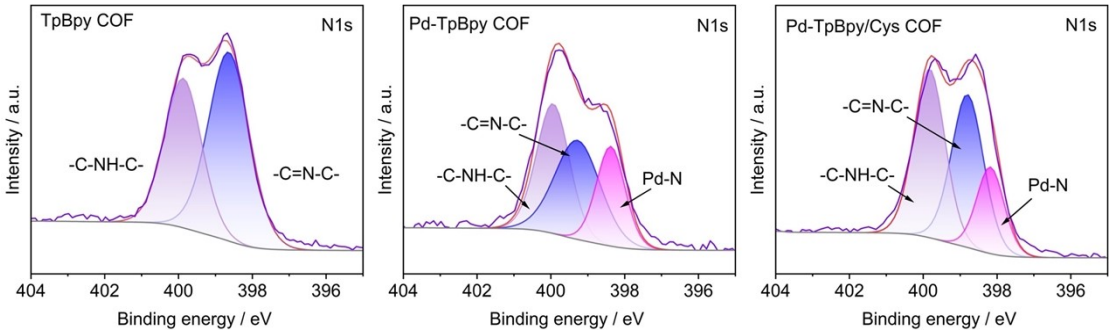

Fig. S9. N 1s XPS spectra of TpBpy COF, Pd-TpBpy COF and Pd-TpBpy/Cys COF.

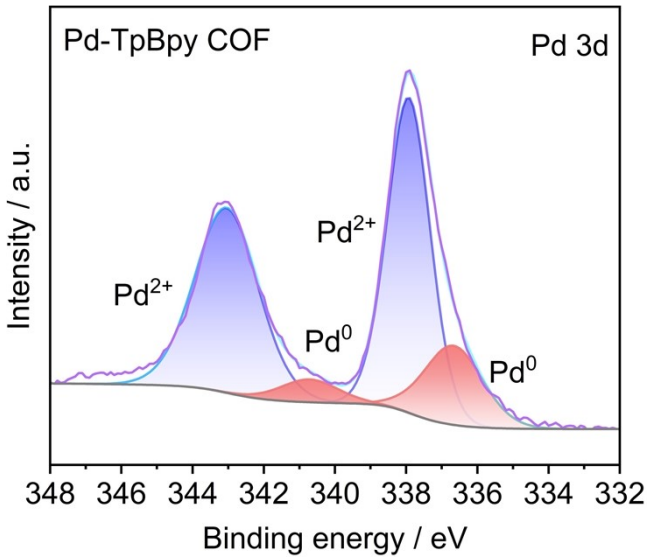

Fig. S10. Pd 3d XPS spectrum of Pd-TpBpy COF after stirring in an EtOH/H_2O mixed solution for 6 h without cysteamine.

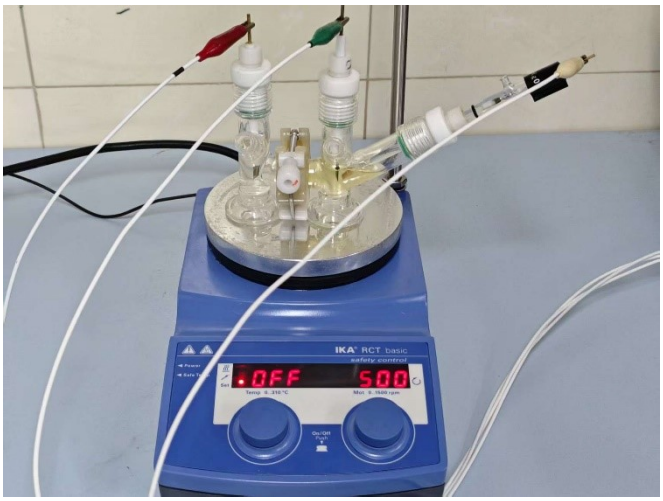

Fig. S11. Reaction setup for electrochemical semi-hydrogenation of alkynes.

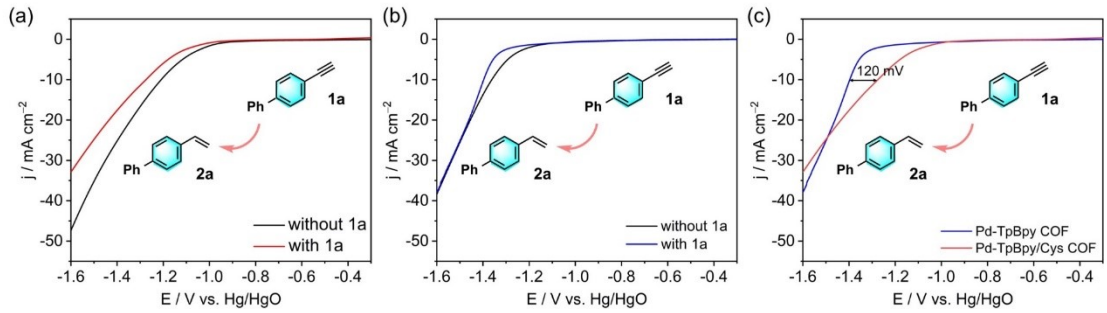

Fig. S12. (a) LSV curves of Pd-TpBpy/Cys COF at a scan rate of 10 mV s^{-1} in 1 M KOH solution (Diox/H_2O, 5:5 v/v) with and without **1a**. (b) LSV curves of Pd-TpBpy COF at a scan rate of 10 mV s^{-1} in 1 M KOH solution (Diox/H_2O, 5:5 v/v) with and without **1a**. (c) LSV curves of Pd-TpBpy/Cys COF and Pd-TpBpy COF at a scan rate of 10 mV s^{-1} with **1a**.

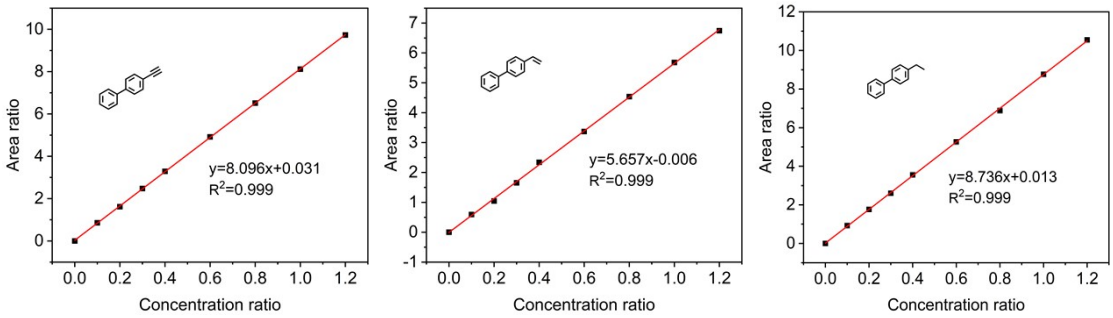

Fig. S13. HPLC calibration curves used for quantifying conversion of the substrate (4-ethynylbiphenyl) and yield of 4-ethenylbiphenyl and 4-ethylbiphenyl with 1-ethylnaphthalene as internal standard.

Table S4. Optimization of Reaction Conditions

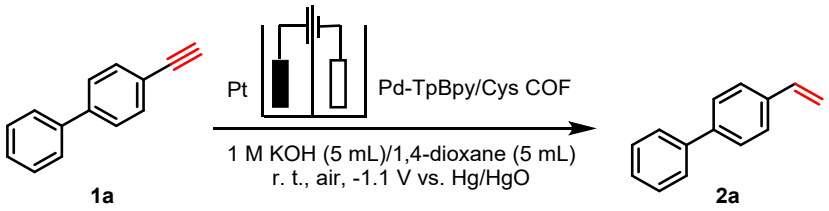

Entry	Variation from standard conditions	Conversion of **1a** (%)	Selectivity of **2a** (%)
1	none	87	97
2	1 M KOH/1,4-dioxane (4:6, v/v)	63	96
3	1 M KOH/1,4-dioxane (6:4, v/v)	70	99
4	No electric current	N.R.	—
5	C paper as the working electrode	N.R.	—
6	$Pd(OAc)_2$ as catalyst, C paper as cathode	98	3

Standard reaction conditions: 4-ethynylbiphenyl (0.1 mmol), Pd-TpBpy/Cys COF working area (1.0 × 1.0 cm^2), 1.0 M KOH/Dioxane (5/5, v/v, 10 mL), room temperature, −1.1 V vs Hg/HgO. Reaction time: 12 h. The conversion of **1a** and the selectivity of **2a** were determined by HPLC.

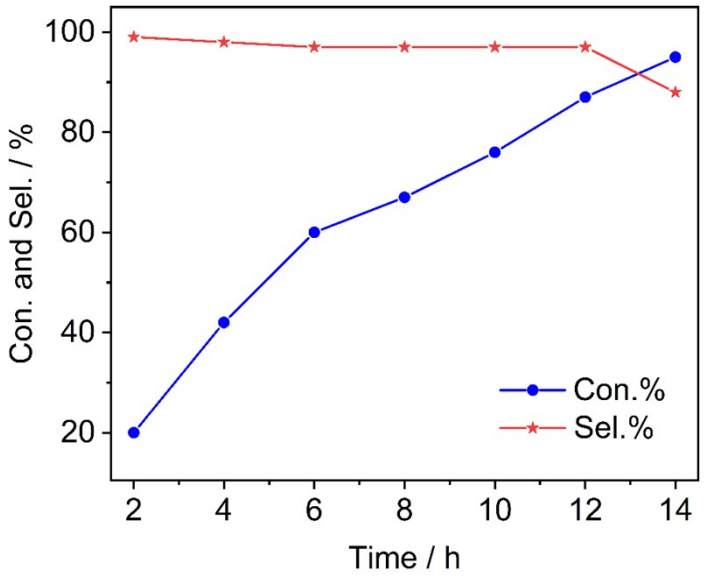

Fig. S14. Time-dependent **1a** conversion (Con.) and **2a** selectivity (Sel.) over Pd-TpBpy/Cys COF.

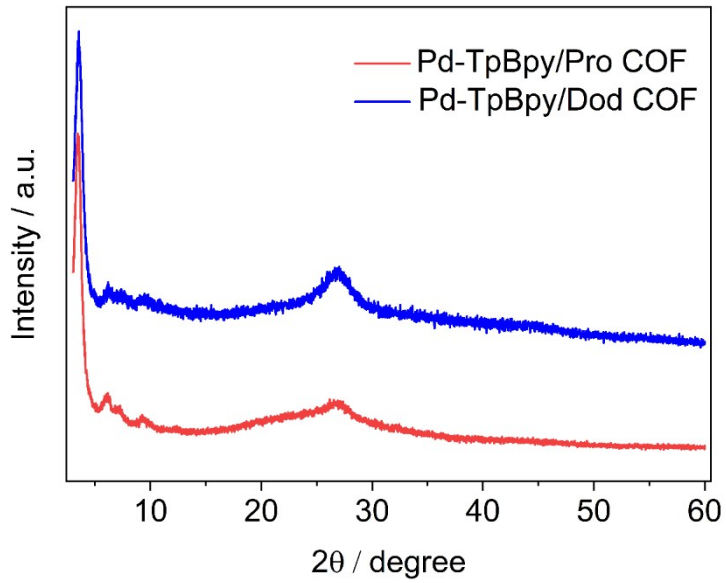

Fig. S15. PXRD patterns of Pd-TpBpy/Pro COF and Pd-TpBpy/Dod COF

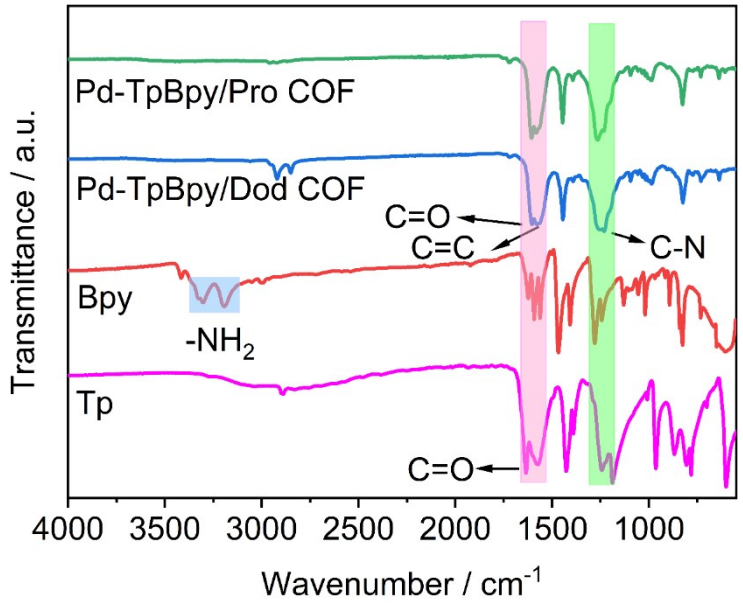

Fig. S16. FT-IR spectra of Tp, Bpy, Pd-TpBpy/Dod COF and Pd-TpBpy/Pro COF.

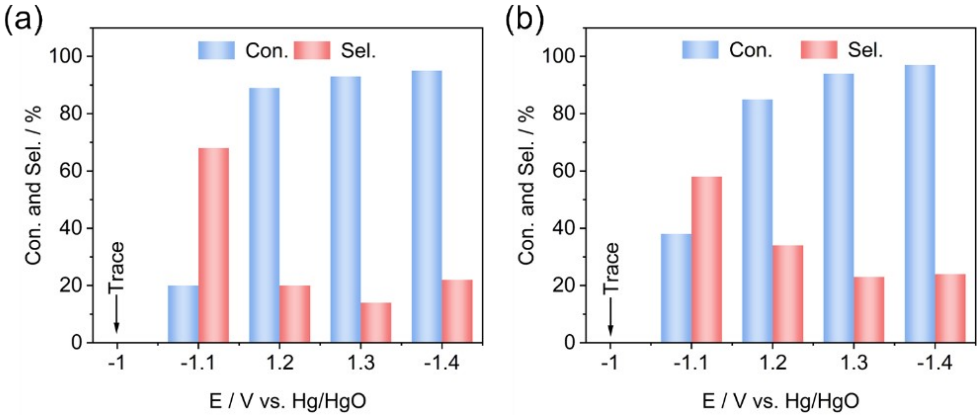

Fig. S17. (a) Potential-dependent conversion of **1a** and selectivity of **2a** over Pd-TpBpy/Pro COF. (b) Potential-dependent conversion of **1a** and selectivity of **2a** over Pd-TpBpy/Dod COF.

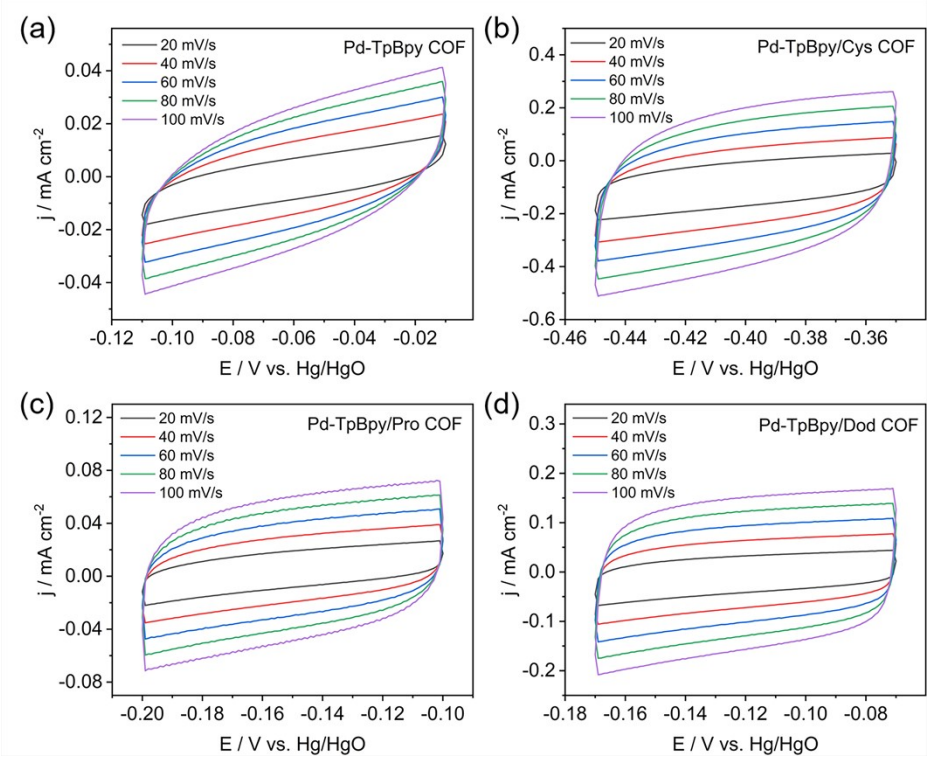

Fig. S18. CV patterns at different scan rates of (a) Pd-TpBpy COF, (b) Pd-TpBpy/Cys COF, (c) Pd-TpBpy/Pro COF, and (d) Pd-TpBpy/Dod COF.

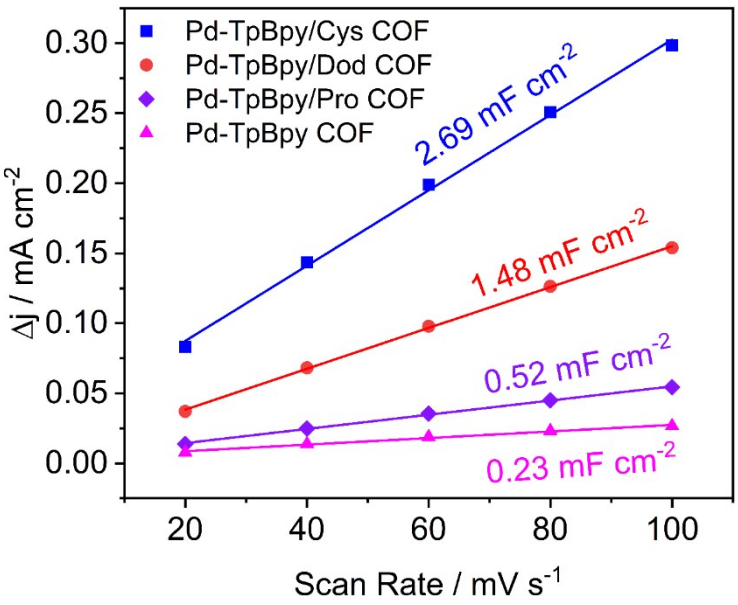

Fig. S19. The double-layer capacitance (Cdl) plots of Pd-TpBpy/Cys COF, Pd-TpBpy/Dod COF, Pd-TpBpy/Pro COF and Pd-TpBpy COF in a three-electrode system.

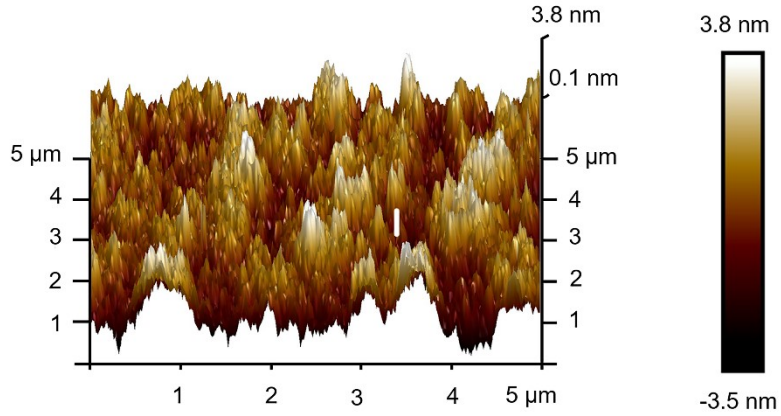

Fig. S20. AFM image of the Pd-TpBpy/Cys COF cathode. (Electrode roughness was 3.8 nm)

Table S5. Calculated electrochemical active surface area (ECSA) and roughness factor (Rf) of Pd-TpBpy/Cys COF cathode.

Entry	Double-layer capacitance (Cdl)	Electrochemical active surface area (ECSA)	Electrode roughness factor (Rf)
1	2.69 mF cm^{-2}	67 cm^{-2}	67

Note: The ECSA was calculated using the equation ECSA = Rf × S. The roughness factor (Rf) is given by Rf = Cdl/Cs, where Cs is the specific double-layer capacitance, referenced from comparable samples as 40 μF·cm^{-2}.[1, 2] S represents the geometric area of the working electrode (1 cm^2).

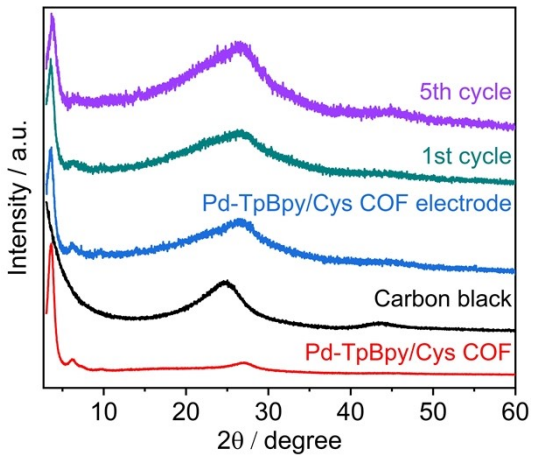

Fig. S21. PXRD patterns of Pd-TpBpy/Cys COF before and after the 1st and 5th cycles.

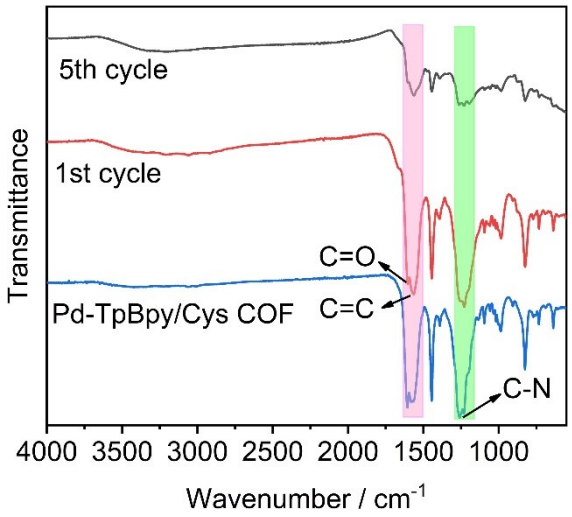

Fig. S22. FT-IR spectra of Pd-TpBpy/Cys COF before and after the 1st and 5th cycles.

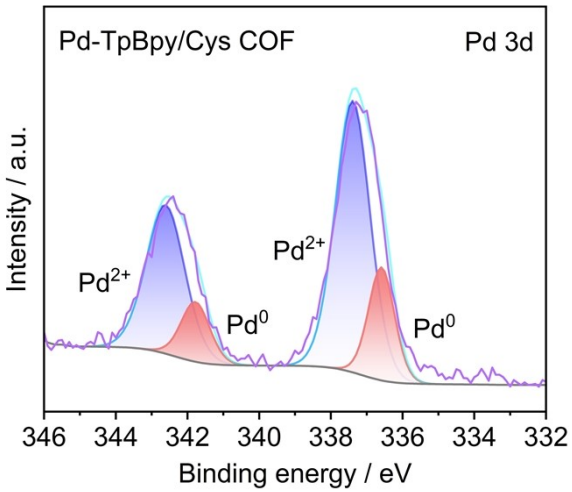

Fig. S23. Pd 3d XPS spectrum of Pd-TpBpy/Cys COF after the catalytic reaction.

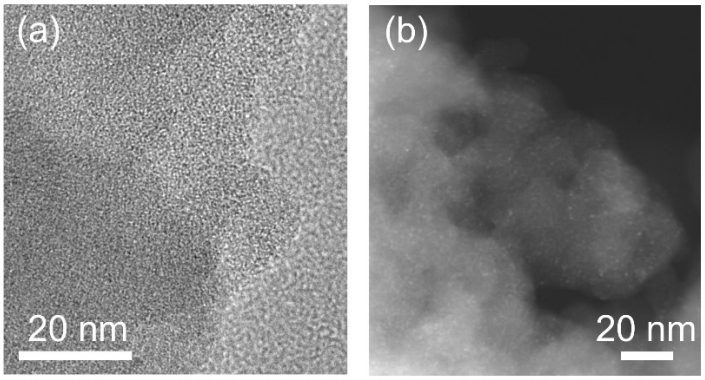

Fig. S24. TEM image (a) and HAADF-STEM image (b) of Pd-TpBpy/Cys COF after the catalytic reaction.

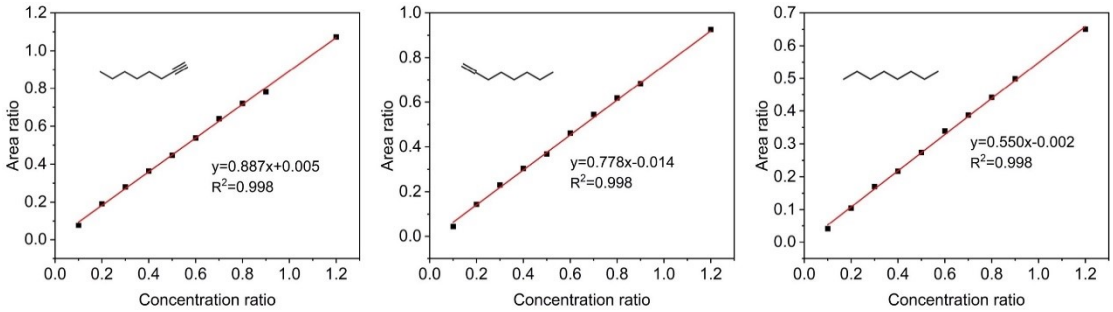

Fig. S25. Gas Chromatography (GC) calibration curves used for quantifying conversion of the substrate (oct-1-yne) and yield of oct-1-ene and octane, with 1,2-dichlorobenzene as the internal standard.

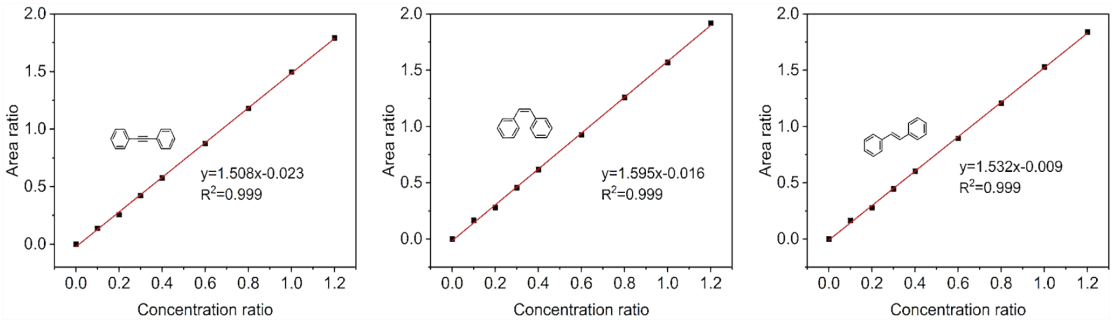

Fig. S26. Gas Chromatography (GC) calibration curves used for quantifying conversion of the substrate (1,2-diphenylethyne) and yield of cis-stilbene and trans-stilbene, with dodecane as internal standard.

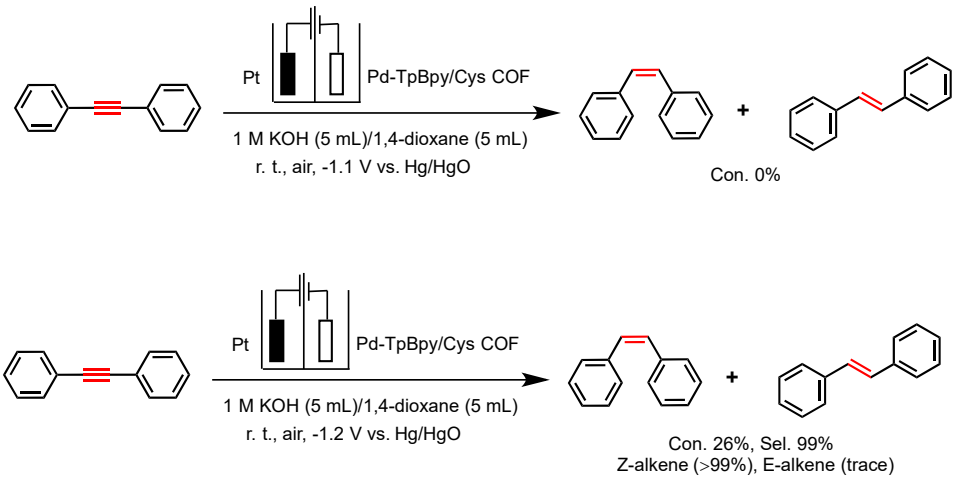

Fig. S27. Electrochemical behavior of 1,2-diphenylacetylene over Pd-TpBpy/Cys COF cathode at the applied potentials of -1.1 V and -1.2 V, respectively.

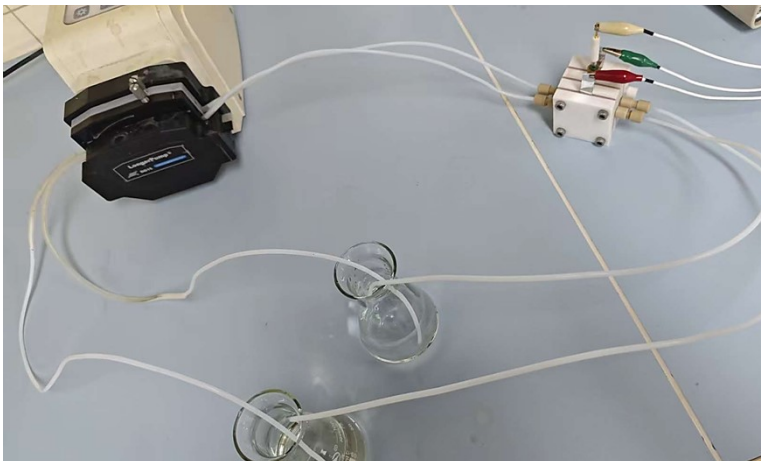

Fig. S28. Electrocatalytic semihydrogenation of 10 mmol **1a** in a continuous-flow electrolyzer. Standard reaction conditions: **1a** (10 mmol), Pd-TpBpy/Cys COF working area (1.0 × 1.0 cm^2), 1.0 M KOH/Dioxane (25/25, v/v, 50 mL), room temperature, −1.1 V vs Hg/HgO. Reaction time: 12 h. The conversion of **1a** and the selectivity of **2a** were determined by HPLC.

In the flow electrolysis cell used for the reaction, the spacing between the working electrode and the counter electrode was 24.34 mm. Both the catholyte and anolyte were circulated at a flow rate of 1 mL/min. The pressure drop was calculated using the Hagen–Poiseuille equation:

$$Q = \frac{\pi \Delta P r^4}{8 \mu L}$$

The value of pressure drop is 18 Pa.

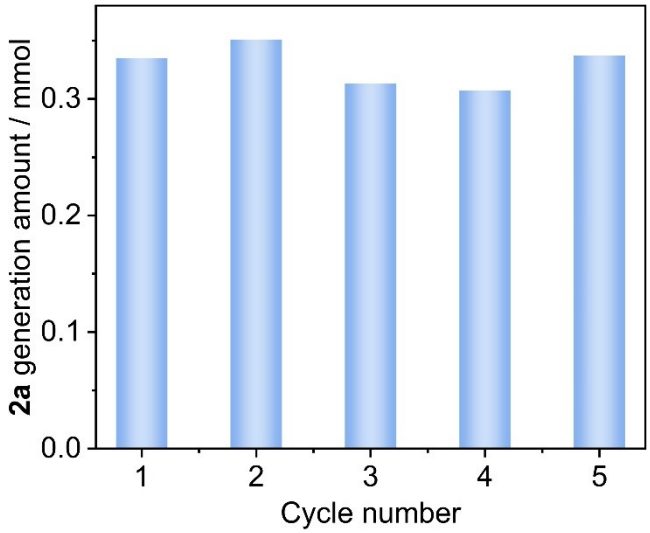

Fig. S29. Cyclic tests for Pd-TpBpy/Cys COF in a continuous-flow electrolyzer (12 h per cycle).

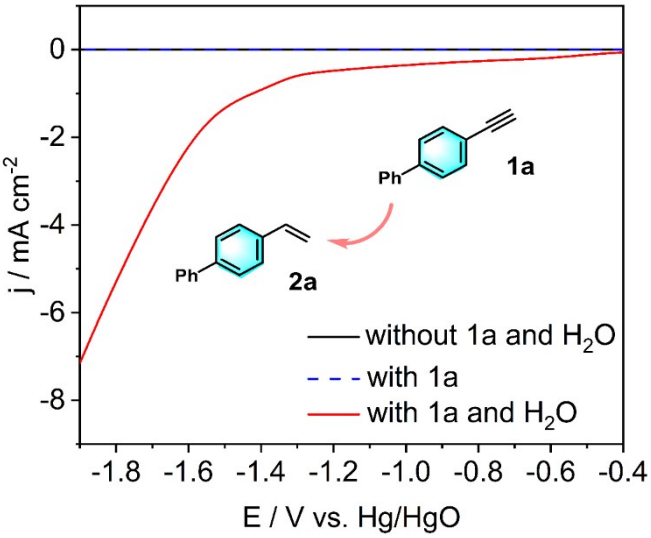

Fig. S30. LSV curves of Pd-TpBpy/Cys COF in a dioxane solution using 0.1 M $LiClO_4$ as the supporting electrolyte.

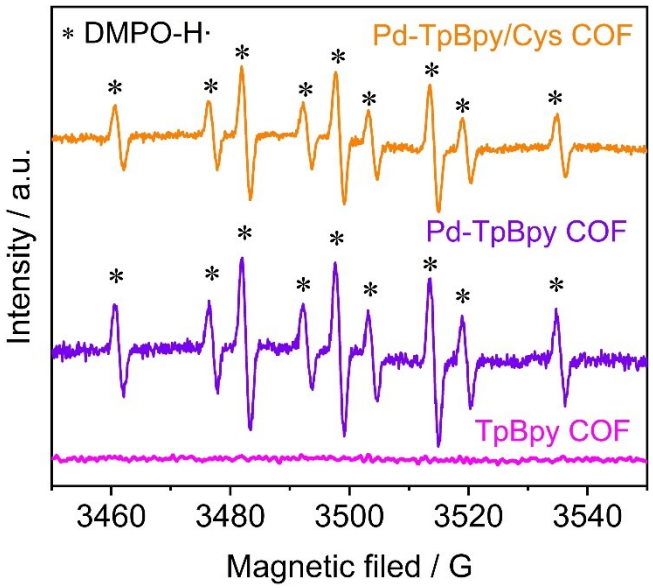

Fig. S31. The control EPR spectra for trapping key intermediate H• under different COFs cathodes.

Table S6. ICP-OES analysis of Pd loading (wt%) of different catalysts.

Different catalysts	Mass fraction of Pd (wt%)
Pd-TpBpy COF	9.43
Pd-TpBpy/Cys COF	2.71

Table S7. ICP-MS analysis of Pd leaching.

Entry	Item	Palladium element content (μg/L)	Pd Leaching Rate
1	Reaction solution of Pd-TpBpy COF in EtOH/H_2O system	1990.22	52.37%
2	Reaction solution of Pd-TpBpy COF in KOH/1,4-dioxane system	796.76	1.68%
3	H-type electrolytic cell reaction solution (Pd-TpBpy/Cys COF as the catalyst）	80.58	0.59%
4	Flow electrolytic cell reaction solution (Pd-TpBpy/Cys COF as the catalyst)	45.22	1.65%

Note: For Entry 1, 2 mg of Pd-TpBpy COF was stirred in an EtOH/H_2O mixture (v/v, 8:2, mL) for 6 hours. After filtration to remove the solid, the resulting filtrate was diluted 5-fold prior to analysis. Entry 2 followed the same procedure, except that 5 mg of catalyst was used and the solvent was a mixture of 1 M KOH and 1,4-dioxane (v/v, 5:5, mL). Entries 3 and 4 were obtained by analyzing the catholyte collected after 12 hours of electrolysis at a constant potential of –1.1 V vs. Hg/HgO (H-type electrolytic cell: the volume of the electrolytic solution was 10 mL; flow electrolytic cell: the volume of the electrolytic solution was 50 mL).

Table S8. Lists the elemental contents of Pd-TpBpy/Cys COF determined by elemental analysis and ICP-OES.

Element	N	C	H	S	O	Pd
Content (wt%)	16.53	58.39	3.62	0.94	19.08	2.71

Based on these elemental content results, the calculated molar ratio of Pd to S is approximately 1:1.15. The loading mass fraction of cysteamine in Pd-TpBpy/Cys COF was further determined to be 2.26 wt% using the following formula:

$$w_{cysteamine}(\%) = \frac{M_{cysteamine}}{M_S} \times w_s(\%)$$

Where $w_{cysteamine}$ represents the mass fraction of cysteamine (wt%), w_s represents the mass fraction of S (wt%), $M_{cysteamine}$ is the molar mass of cysteamine (g/mol), Ms is the atomic weight of sulfur (g/mol).

Table S9. Control Experiment Results

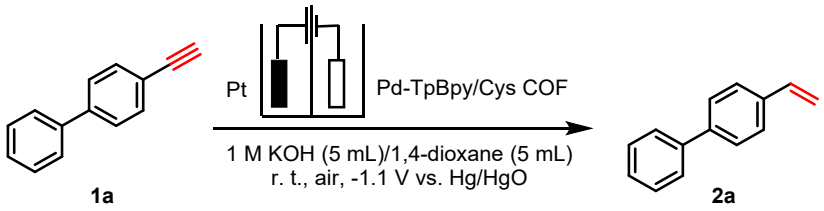

Entry	Variation from standard conditions	Conversion of **1a** (%)	Selectivity of **2a** (%)
1	Without H_2O, 0.1 M $LiClO_4$/Dioxane	N.R.	—
2	With H_2O, 0.1 M $LiClO_4$/Dioxane	65	95
3	No electric current and H_2 atmosphere	N.R.	—

Standard reaction conditions: 4-ethynylbiphenyl (0.1 mmol), Pd-TpBpy/Cys COF working area (1.0 × 1.0 cm^2), 1.0 M KOH/Dioxane (5/5, v/v, 10 mL), room temperature, −1.1 V vs Hg/HgO. Reaction time: 12 h. The conversion of **1a** and the selectivity of **2a** were determined by HPLC.

Table S10. Change in pH before and after the reaction.

Entry	Item	Before reaction	After 12 h of reaction
1	Deionized water	7.00	—
2	Anode pH (with aqueous KOH as the electrolyte)	13.98	13.65
3	Cathode pH (with aqueous KOH as the electrolyte)	14.00	14.32
4	Anode pH (with $LiClO_4$ as the electrolyte)	7.10	2.10
5	Cathode pH (with $LiClO_4$ as the electrolyte)	7.00	11.82

A slight pH change ($\Delta pH \approx 0.3$ units) in the anode/cathode compartment under the optimized reaction conditions were detected (Table S10, entries 2 and 3), which might be attributed to the fact that 1.0 M KOH was a high-concentration alkali solution with a certain buffering capacity. Replacing KOH with $LiClO_4$, the solutions of the anode and cathode became acidic and alkaline, respectively (Table S10, entries 4 and 5). These results demonstrated that no obvious pH crossover under the reaction conditions.

Section 4. NMR data (^{1}H NMR and ^{13}C NMR spectra)

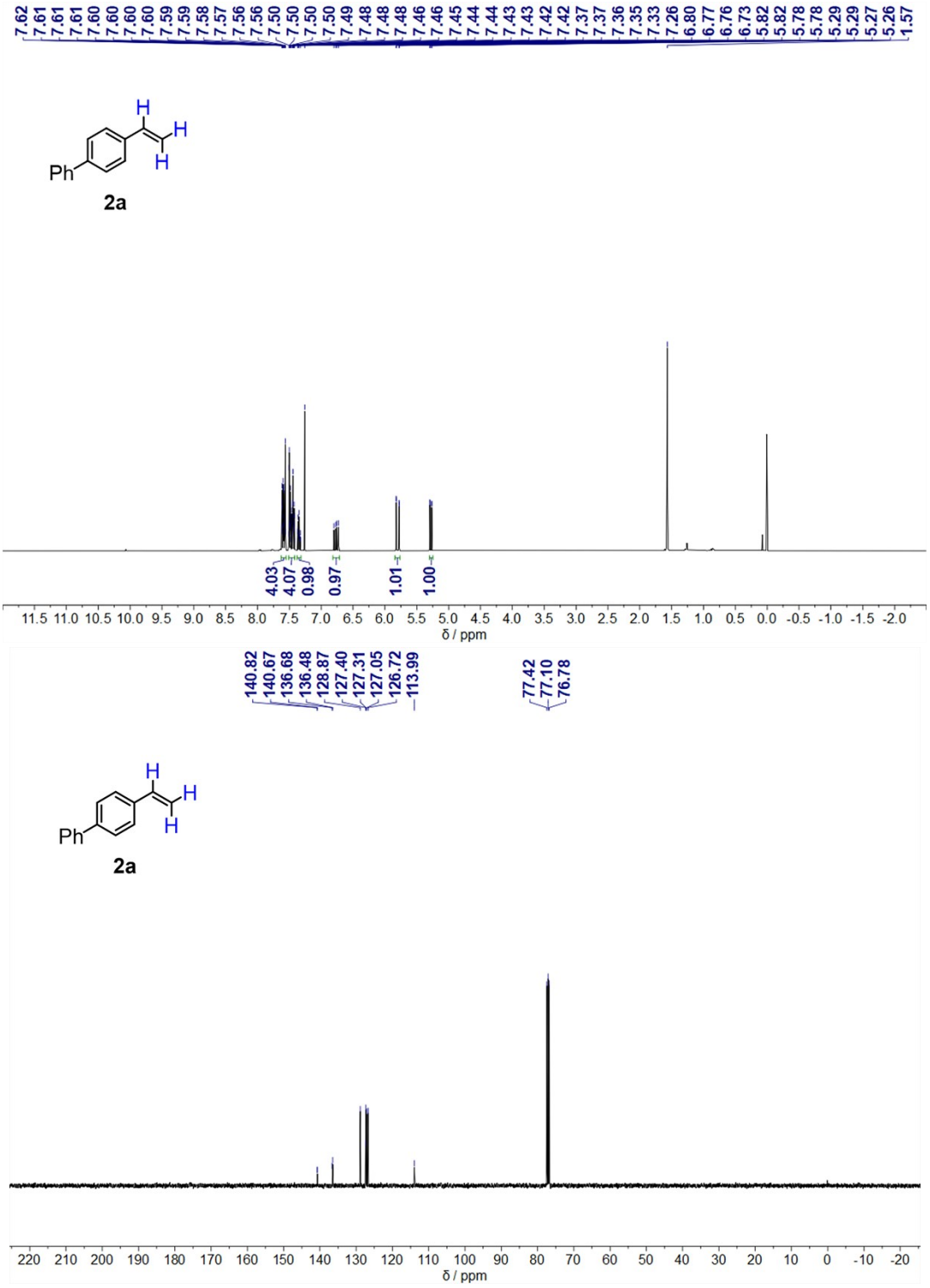

Fig. S32. ^{1}H NMR (400 MHz, Chloroform-d) δ [ppm] 7.62–7.55 (m, 4H), 7.51–7.42 (m, 4H), 7.35 (tt, *J* = 7.6, 1.6 Hz, 1H), 6.77 (dd, *J* = 17.6, 10.8 Hz, 1H), 5.80 (dd, *J* = 17.6, 0.8 Hz, 1H), 5.28 (dd, *J* = 10.8, 0.8 Hz, 1H). **^{13}C NMR** (101 MHz, Chloroform-d) δ [ppm] 140.82, 140.67, 136.68, 136.48, 128.87, 127.40, 127.31, 127.05, 126.72, 113.99. GC-MS (EI): *m/z* = 180.0 [M^{+}], and theoretical value for $C_{14}H_{12}$ is 180.1.

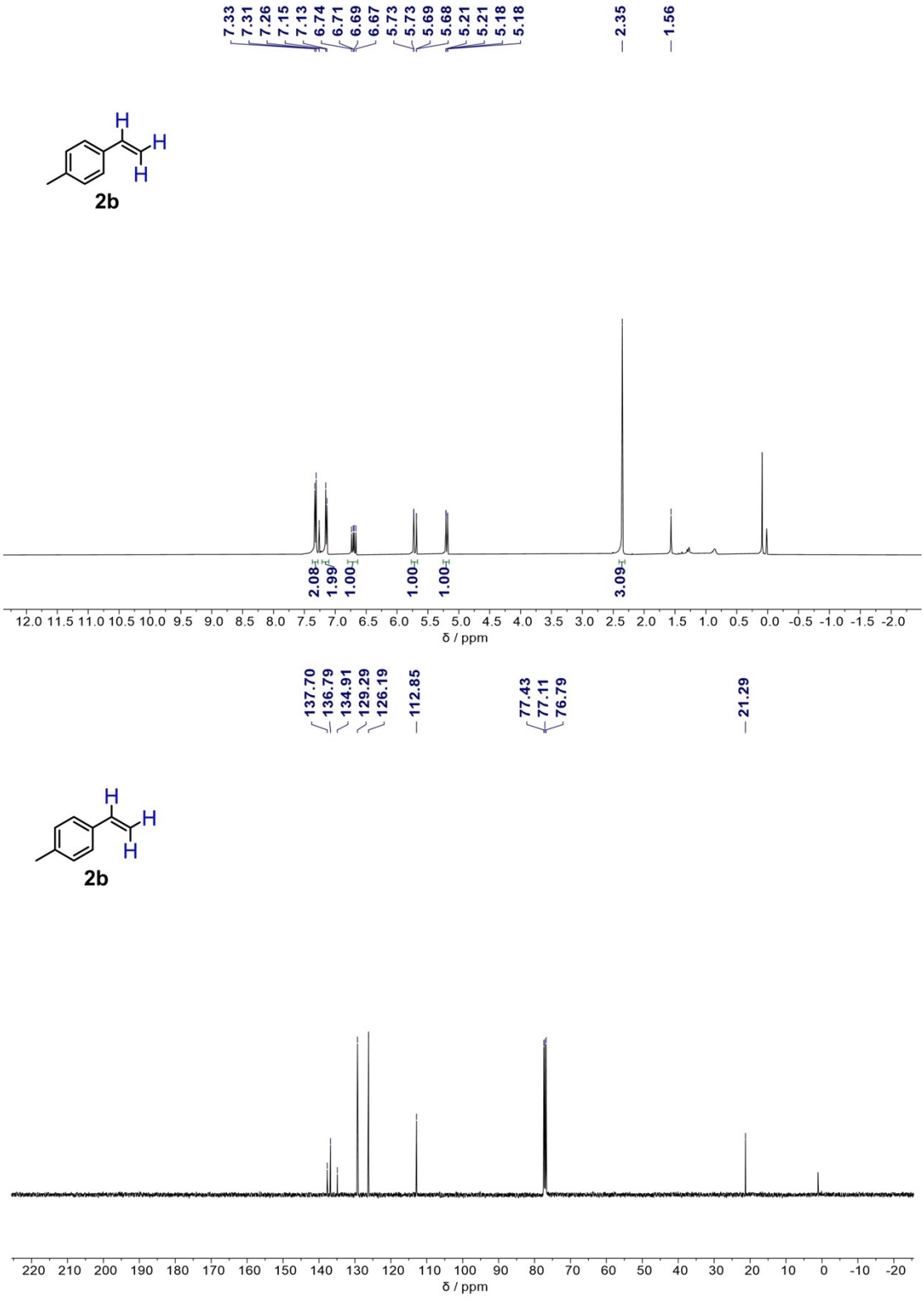

Fig. S33. **^{1}H NMR** (400 MHz, Chloroform-d) δ [ppm] 7.32 (d, *J* = 8.0 Hz, 2H), 7.14 (d, *J* = 8.0 Hz, 2H), 6.70 (dd, *J* = 17.6, 10.8 Hz, 1H), 5.71 (dd, *J* = 17.6, 1.2 Hz, 1H), 5.19 (dd, *J* = 10.8, 1.2 Hz, 1H), 2.35 (s, 3H). **^{13}C NMR** (101 MHz, Chloroform-d) δ [ppm] 137.70, 136.79, 134.91, 129.29, 126.19, 112.85, 21.29. GC-MS (EI): *m/z* = 118.1 [M^{+}], and theoretical value for C_9H_{10} is 118.1

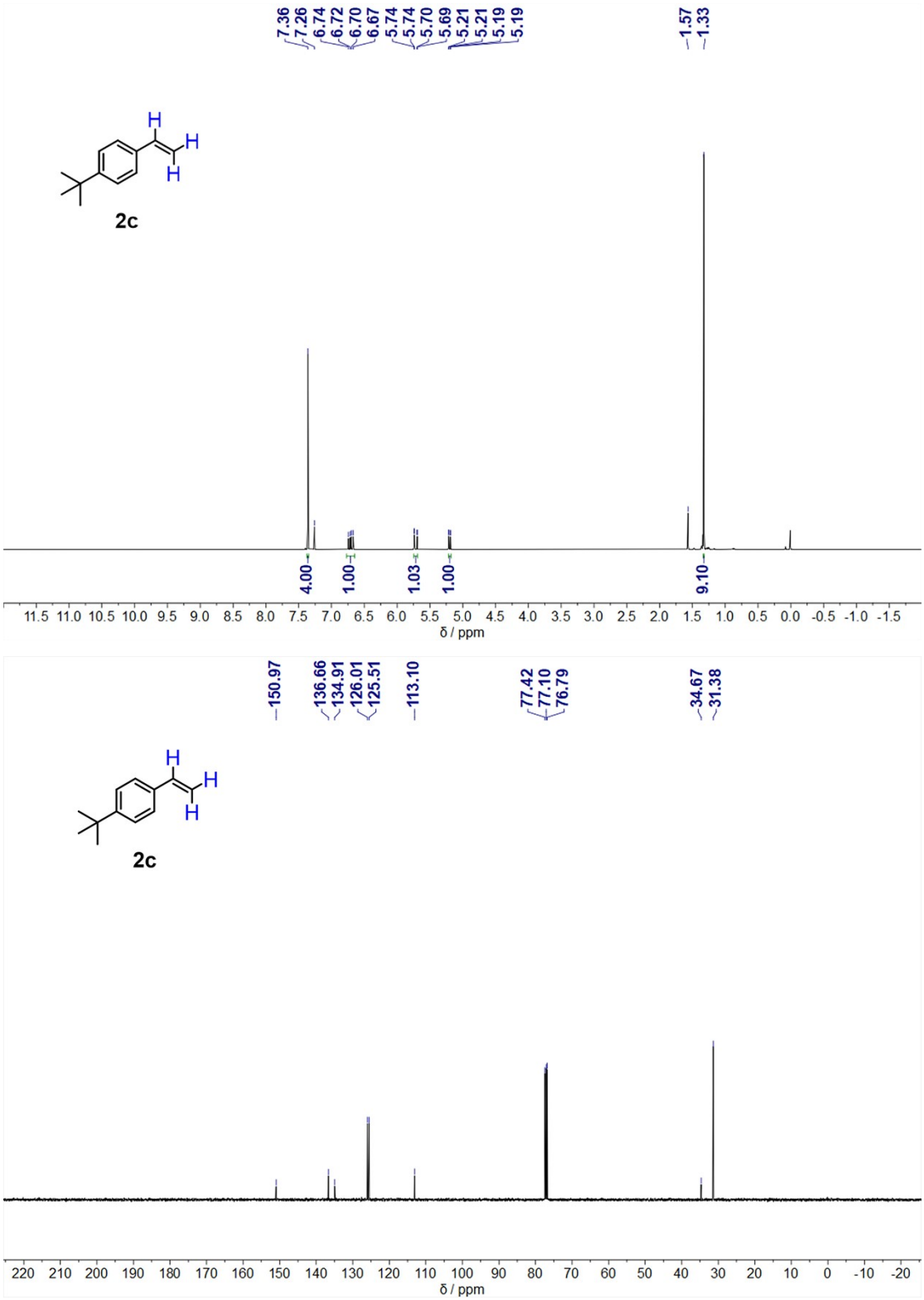

Fig. S34. **^{1}H NMR** (400 MHz, Chloroform-d) δ [ppm] 7.36 (s, 4H), 6.71 (dd, *J* = 17.6, 10.8 Hz, 1H), 5.72 (dd, *J* = 17.6, 0.8 Hz, 1H), 5.20 (dd, *J* = 10.8, 1.2 Hz, 1H), 1.33 (s, 9H). **^{13}C NMR** (101 MHz, Chloroform-d) δ 150.97, 136.66, 134.91, 126.01, 125.51, 113.10, 34.67, 31.38. GC-MS (EI): *m/z* = 160.2 [M^{+}], and theoretical value for $C_{12}H_{16}$ is 160.1.

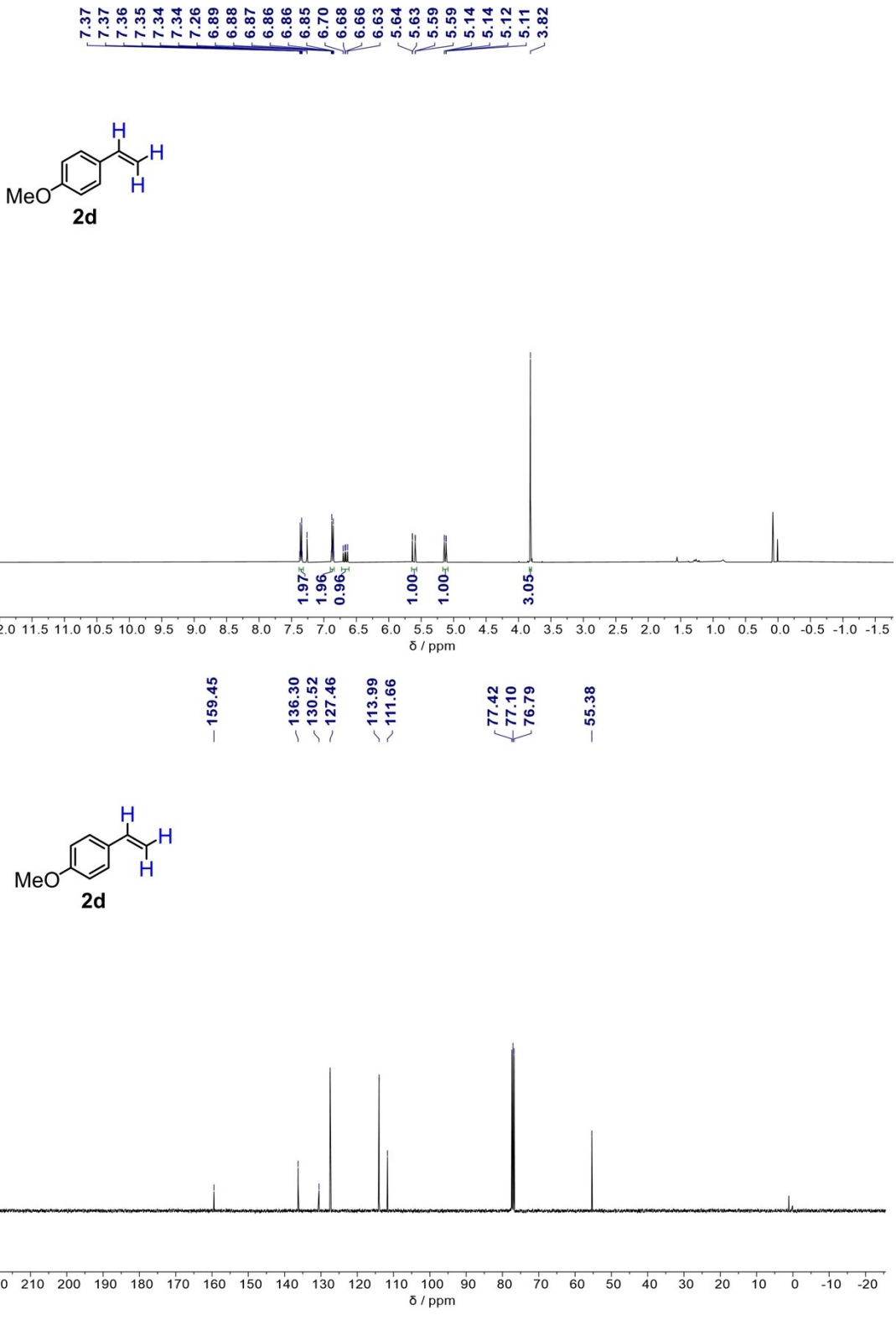

Fig. S35. **^{1}H NMR** (400 MHz, Chloroform-d) δ [ppm] 7.35 (dt, *J* = 9.2, 2.4 Hz, 2H), 6.87 (dt, *J* = 9.2, 2.4 Hz, 2H), 6.67 (dd, *J* = 17.6, 11.2 Hz, 1H), 5.61 (dd, *J* = 17.6, 0.8 Hz, 1H), 5.13 (dd, *J* = 11.2, 0.8 Hz, 1H), 3.82 (s, 3H). **^{13}C NMR** (101 MHz, Chloroform-d) δ [ppm] 159.45, 136.30, 130.52, 127.46, 113.99, 111.66, 55.38. GC-MS (EI): *m/z* = 134.1 [M^{+}], and theoretical value for $C_9H_{10}O$ is 134.1

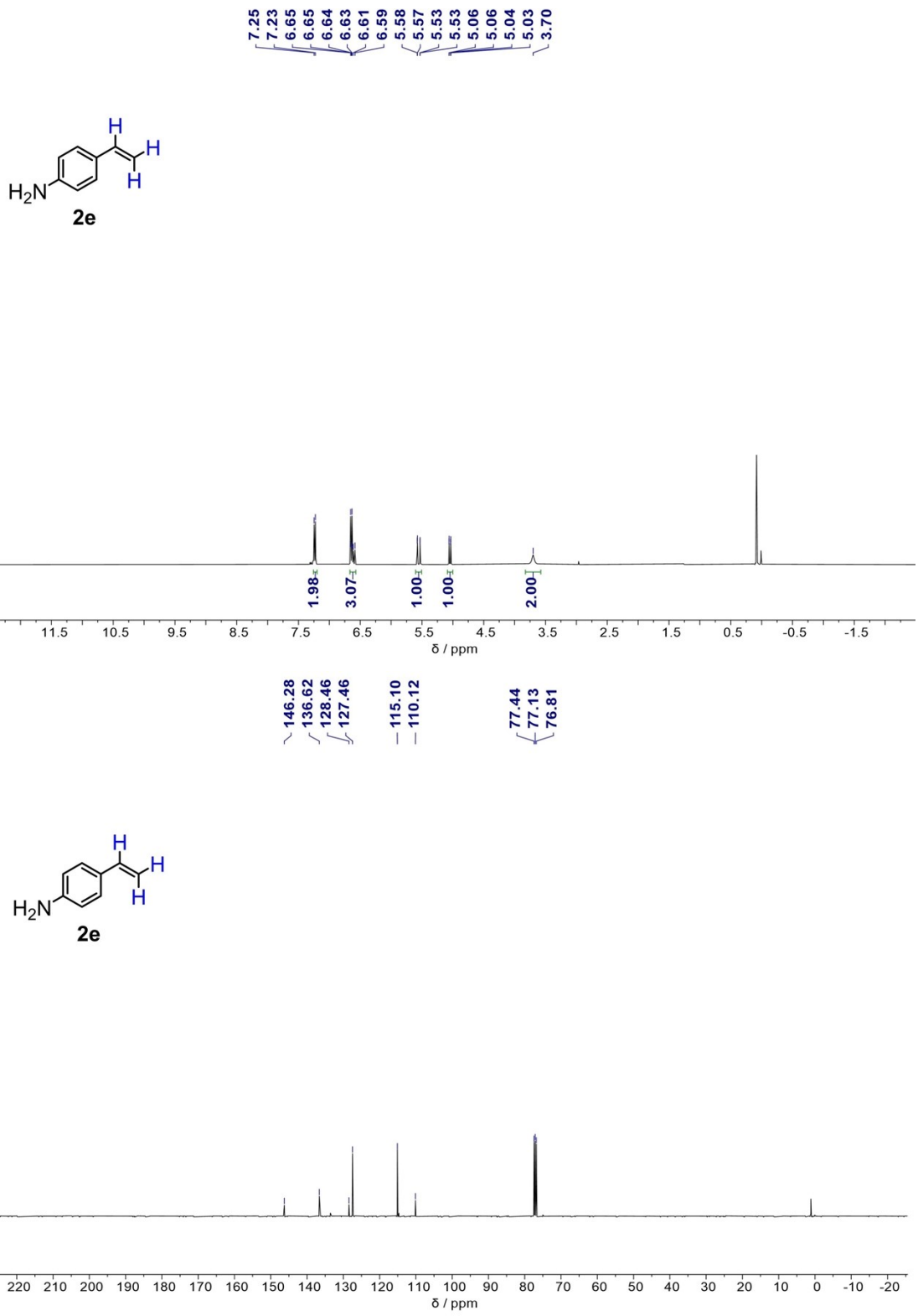

Fig. S36. **^{1}H NMR** (400 MHz, Chloroform-d) δ [ppm] 7.24 (d, *J* = 8.4 Hz, 2H), 6.67–6.57 (m, 3H), 5.55 (dd, *J* = 17.6, 1.2 Hz, 1H), 5.05 (dd, *J* = 10.8, 0.8 Hz, 1H), 3.70 (s, 2H). **^{13}C NMR** (101 MHz, Chloroform-d) δ [ppm] 146.28, 136.62, 128.46, 127.46, 115.10, 110.12. GC-MS (EI): *m/z* = 119.1 [M^+], and theoretical value for C_8H_9N is 119.1

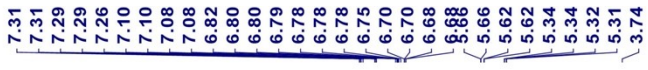

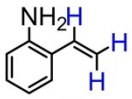

2f

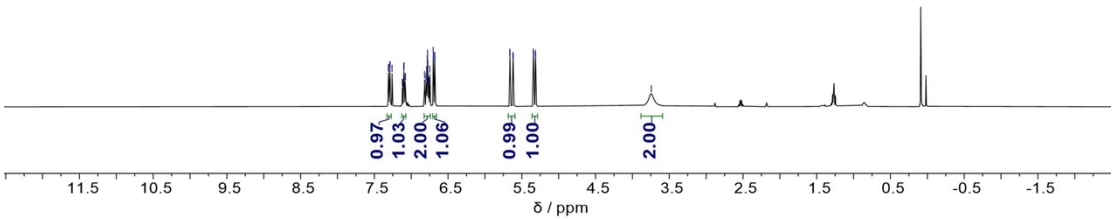

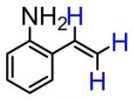

2f

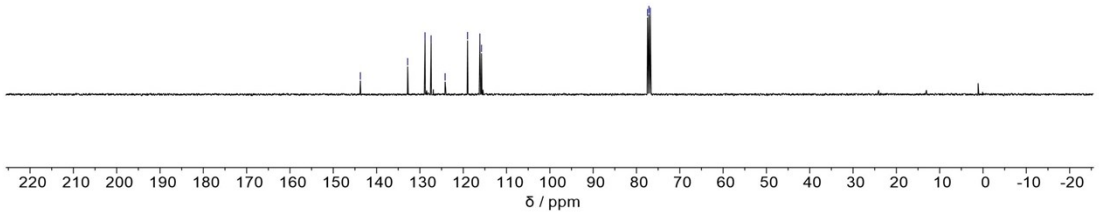

Fig. S37. ^{1}H NMR (400 MHz, Chloroform-d) δ [ppm] 7.30 (dd, *J* = 7.6, 1.6 Hz, 1H), 7.10 (td, *J* = 7.6, 1.6 Hz, 1H), 6.82–6.74 (m, 2H), 6.69 (dd, *J* = 7.8, 1.6 Hz, 1H), 5.64 (dd, *J* = 17.6, 1.2 Hz, 1H), 5.33 (dd, *J* = 11.2, 1.6 Hz, 1H), 3.74 (s, 2H). **^{13}C NMR** (101 MHz, Chloroform-d) δ [ppm] 143.74,132.82, 128.82, 127.42, 124.18,119.01, 116.16, 115.78. GC-MS (EI): *m/z* = 119.1 [M^+], and theoretical value for C_8H_9N is 119.1.

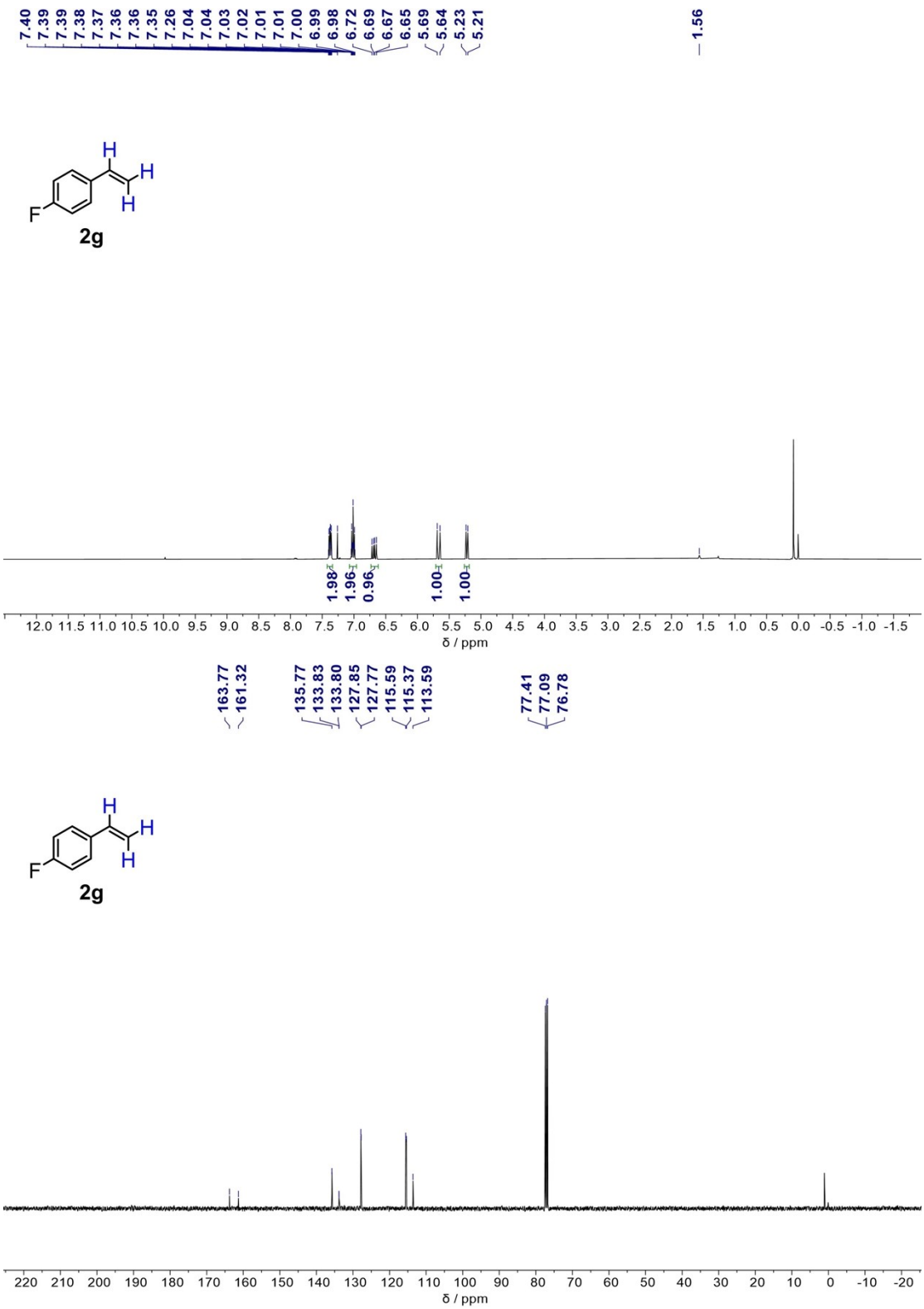

Fig. S38. **^{1}H NMR** (400 MHz, Chloroform-d) δ [ppm] 7.42–7.34 (m, 2H), 7.07–6.96 (m, 2H), 6.68 (dd, *J* = 17.6, 10.8 Hz, 1H), 5.67 (d, *J* = 17.6 Hz, 1H), 5.22 (d, *J* = 10.8 Hz, 1H). **^{13}C NMR** (101 MHz, Chloroform-d) δ [ppm] 162.55 (d, *J* = 247.5 Hz), 135.77, 133.82 (d, *J* = 3.0 Hz), 127.81 (d, *J* = 8.1 Hz), 115.48 (d, *J* = 22.2 Hz), 113.59. GC-MS (EI): *m/z* = 122.1 [M^{+}], and theoretical value for C_8H_7F is 122.1.

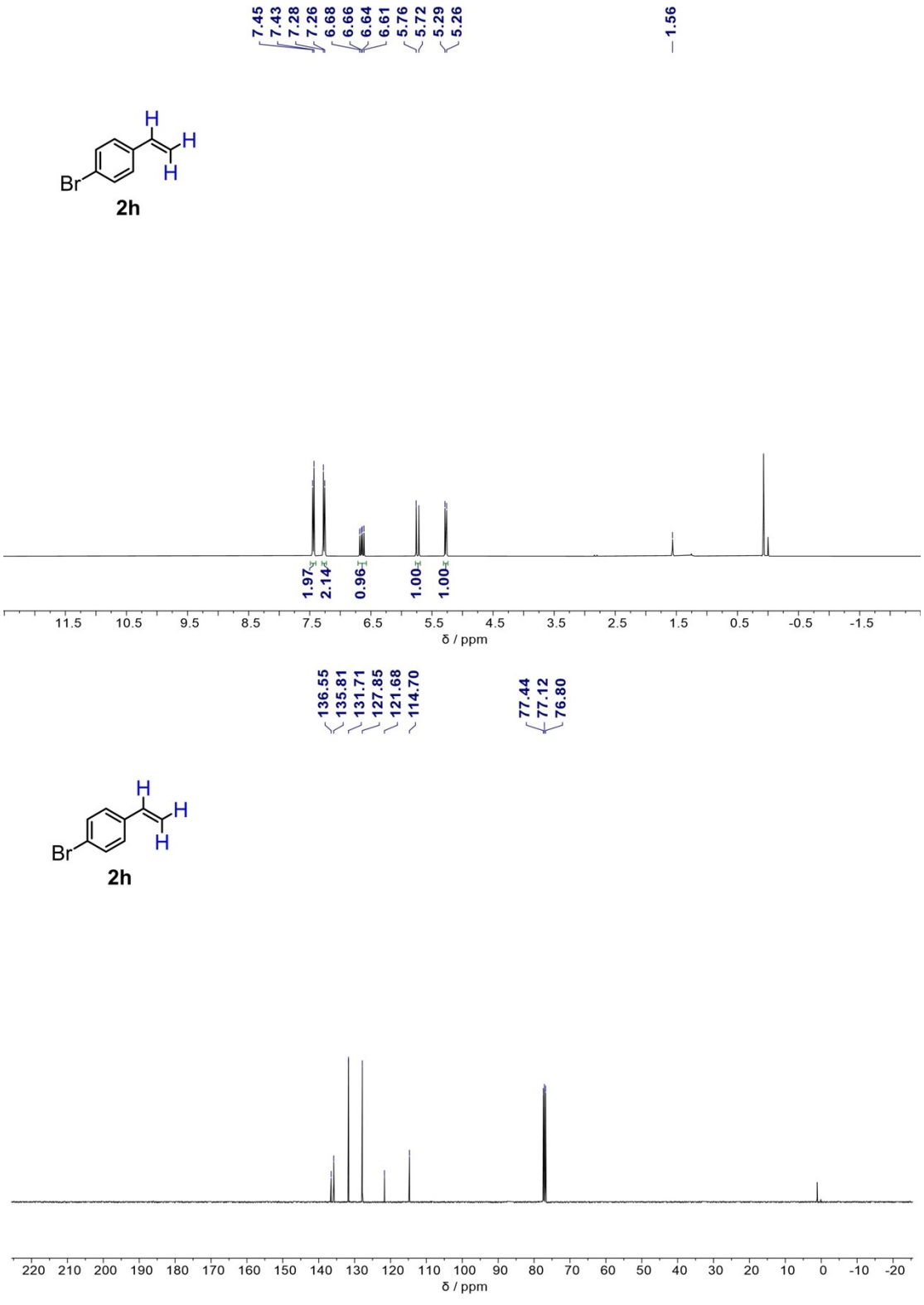

Fig. S39. ^{1}H NMR (400 MHz, Chloroform-d) δ [ppm] 7.44 (d, *J* = 8.4 Hz, 2H), 7.27 (d, *J* = 8.4 Hz, 2H), 6.65 (dd, *J* = 17.6, 10.8 Hz, 1H), 5.74 (d, *J* = 17.6 Hz, 1H), 5.27 (d, *J* = 10.8 Hz, 1H). **^{13}C NMR** (101 MHz, Chloroform-d) δ [ppm] 136.55, 135.81, 131.71, 127.85, 121.68, 114.70. GC-MS (EI): *m/z* = 182.0, 184.0 [M^+], and theoretical value for C_8H_7Br is 182.0, 184.0.

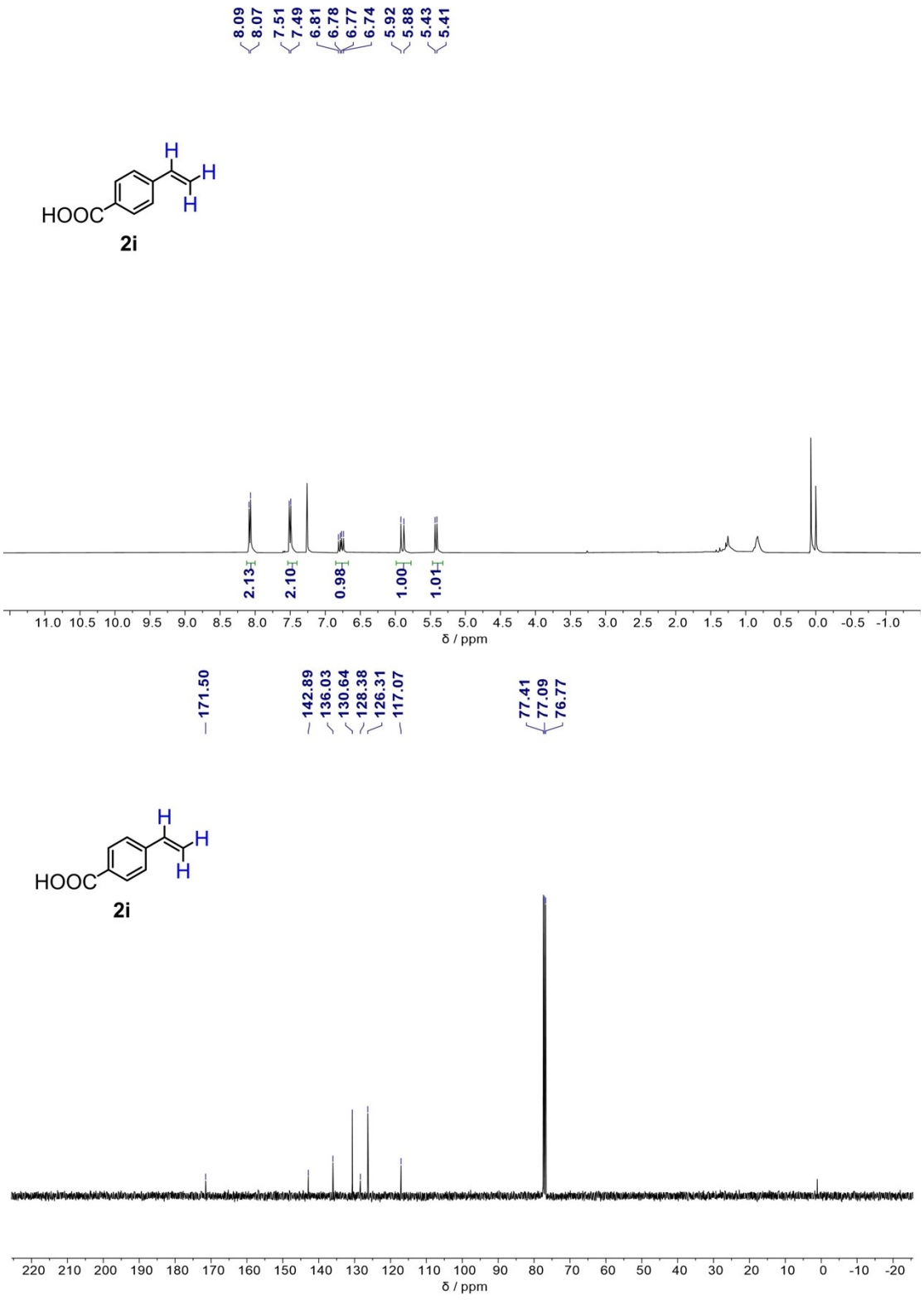

Fig. S40. **^{1}H NMR** (400 MHz, Chloroform-d) δ [ppm] 8.08 (d, *J* = 8.4 Hz, 2H), 7.50 (d, *J* = 8.4 Hz, 2H), 6.78 (dd, *J* = 17.6, 10.8 Hz, 1H), 5.90 (d, *J* = 17.6 Hz, 1H), 5.42 (d, *J* = 10.8 Hz, 1H). **^{13}C NMR** (101 MHz, Chloroform-d) δ [ppm] 171.50, 142.89, 136.03, 130.64, 128.38, 126.31, 117.07. GC-MS (EI): *m/z* = 148.1 [M^+], and theoretical value for $C_9H_8O_2$ is 148.1.

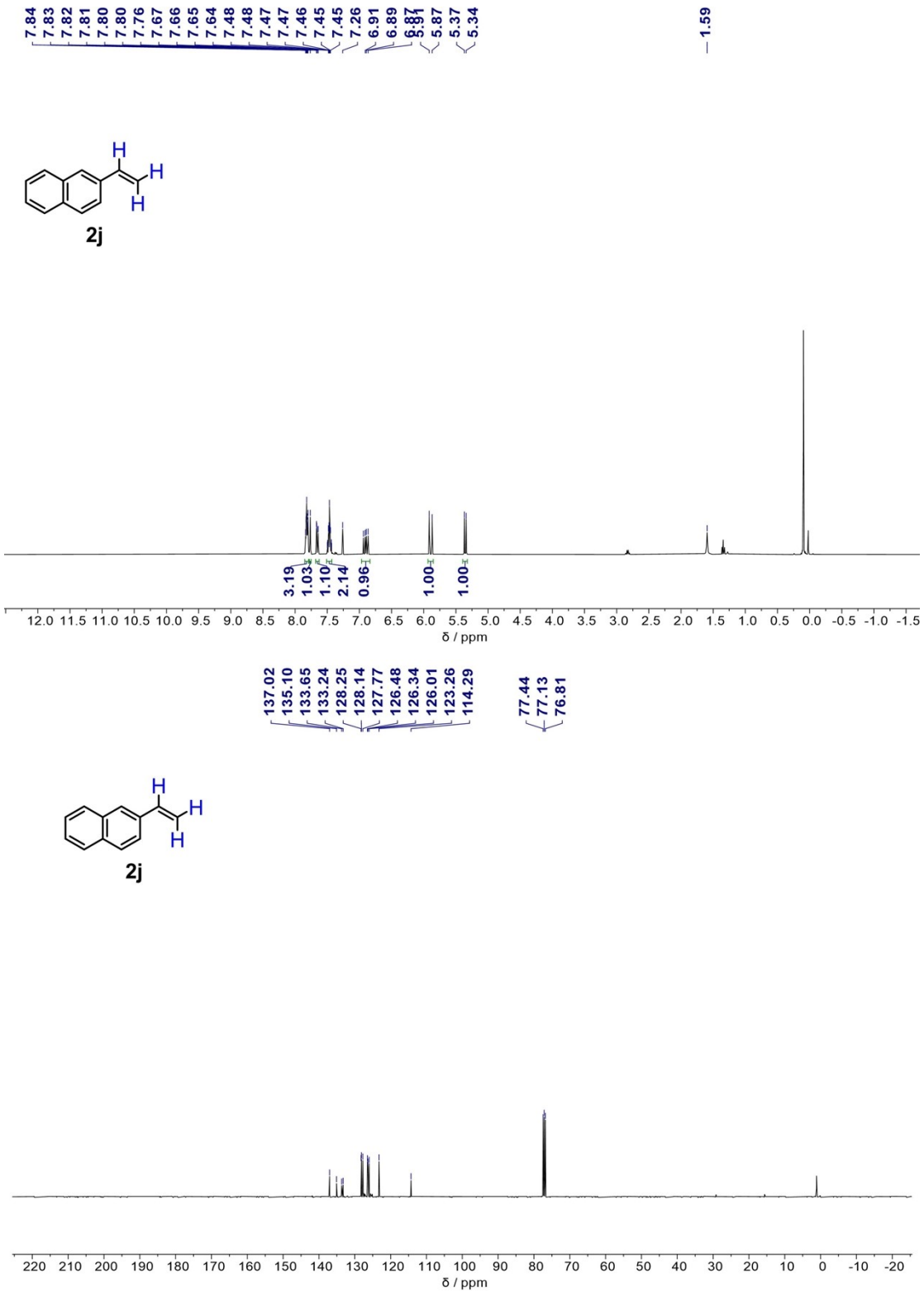

Fig. S41. **^{1}H NMR** (400 MHz, Chloroform-d) δ [ppm] 7.85–7.79 (m, 3H), 7.76 (s, 1H), 7.65 (dd, *J* = 8.6, 2.0 Hz, 1H), 7.51–7.43 (m, 2H), 6.90 (dd, *J* = 17.6, 10.8 Hz, 1H), 5.89 (d, *J* = 17.6 Hz, 1H), 5.35 (d, *J* = 10.8 Hz, 1H). **^{13}C NMR** (101 MHz, Chloroform-d) δ [ppm] 137.02, 135.10, 133.65, 133.24, 128.25, 128.14, 127.77, 126.48, 126.34, 126.01, 123.26, 114.29. GC-MS (EI): *m/z* = 154.1 [M^{+}], and theoretical value for $C_{12}H_{10}$ is 154.1.

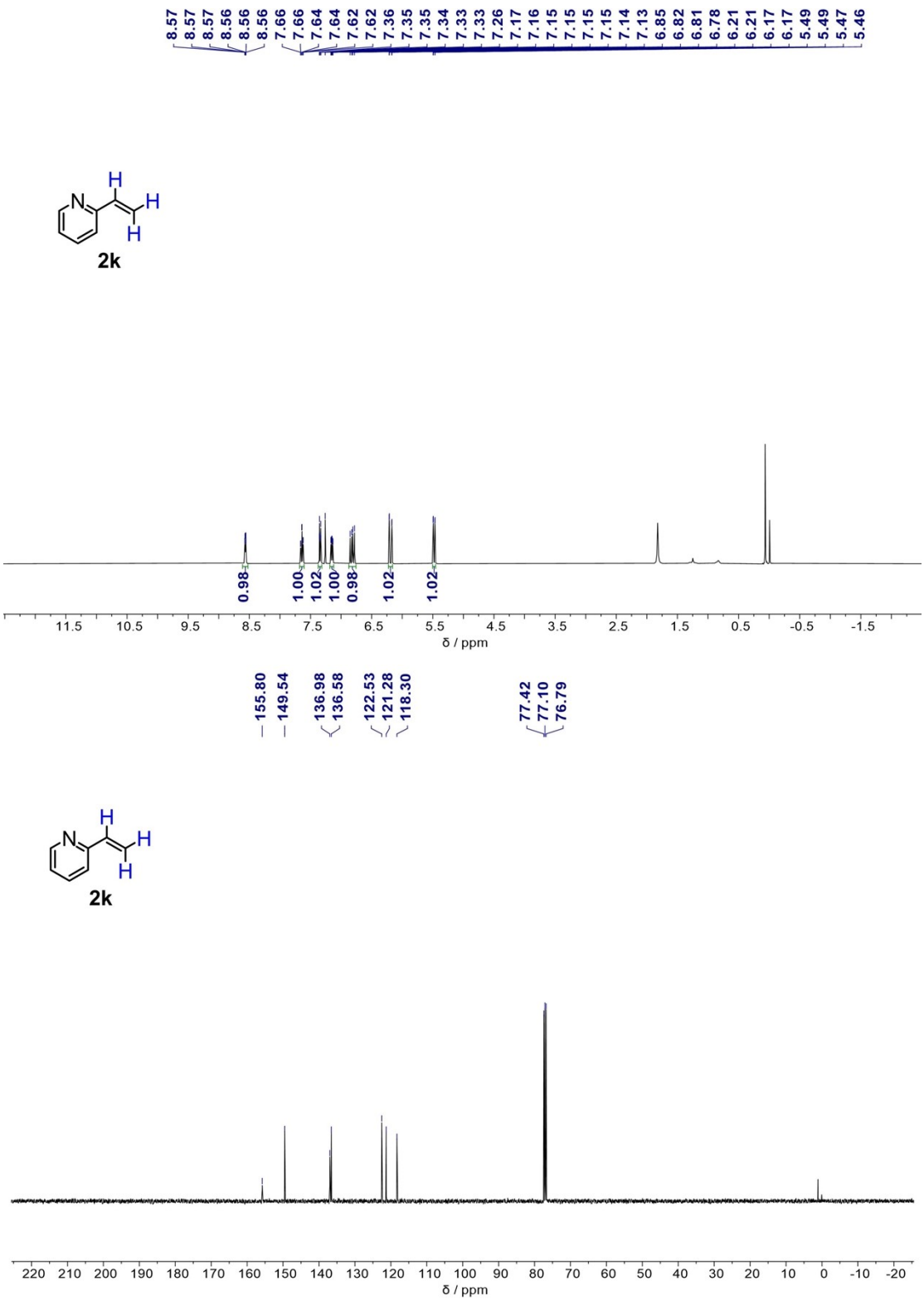

Fig. S42. ^{1}H NMR (400 MHz, Chloroform-d) δ [ppm] 8.61–8.52 (m, 1H), 7.64 (td, *J* = 7.6, 2.0 Hz, 1H), 7.34 (dt, *J* = 8.0, 1.2 Hz, 1H), 7.15 (ddd, *J* = 7.6, 4.8, 1.2 Hz, 1H), 6.82 (dd, *J* = 17.6, 10.8 Hz, 1H), 6.19 (dd, *J* = 17.6, 1.2 Hz, 1H), 5.48 (dd, *J* = 10.8, 1.2 Hz, 1H). **^{13}C NMR** (101 MHz, Chloroform-d) δ [ppm] 155.80, 149.54, 136.98, 136.58, 122.53, 121.28, 118.30. GC-MS (EI): *m/z* = 105.1 [M^{+}], and theoretical value for C_7H_7N is 105.1.

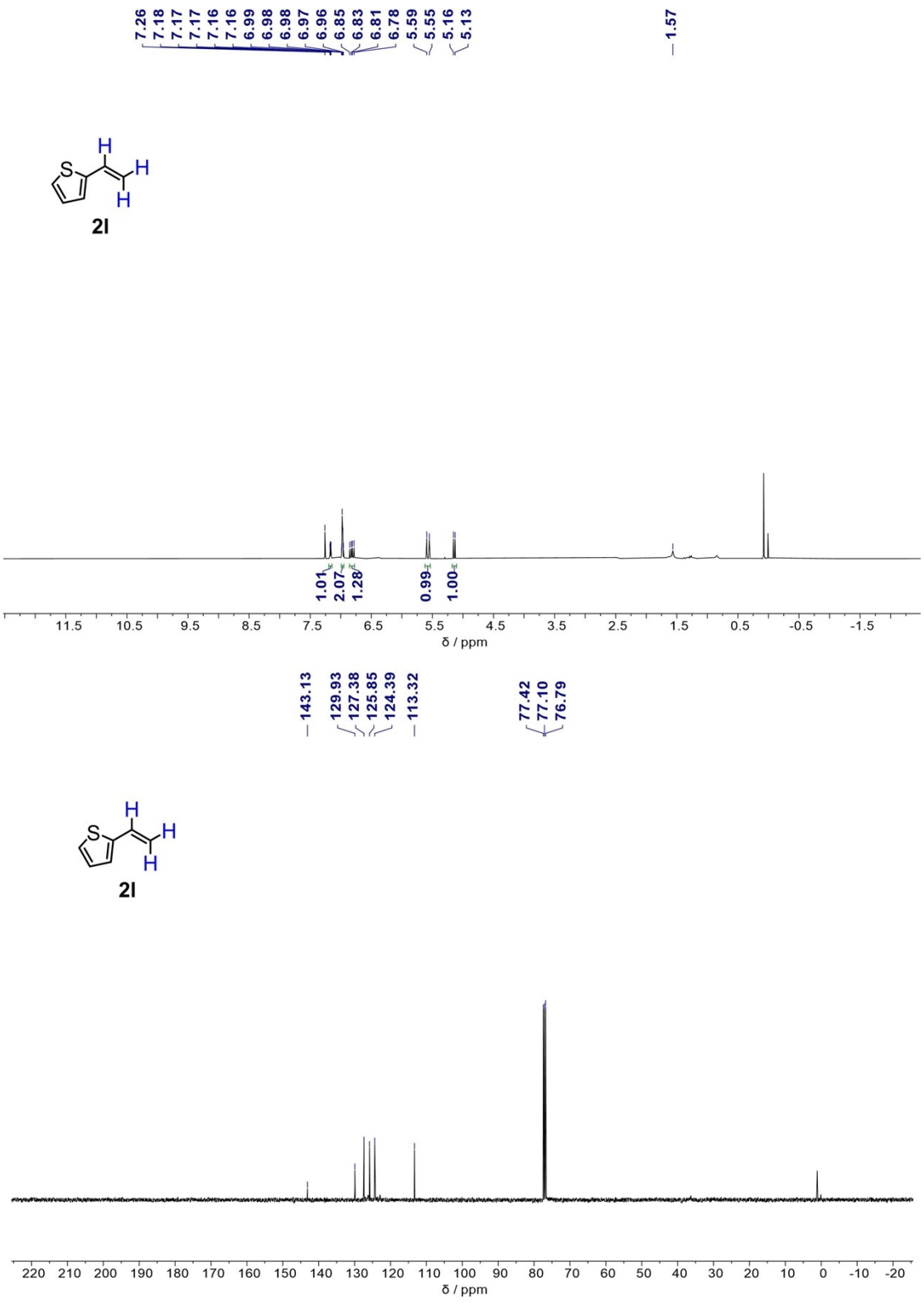

Fig. S43. ^{1}H NMR (400 MHz, Chloroform-d) δ [ppm] 7.19–7.14 (m, 1H), 6.99–6.95 (m, 2H), 6.82 (dd, J = 17.2, 10.8 Hz, 1H), 5.57 (d, J = 17.2 Hz, 1H), 5.14 (d, J = 10.8 Hz, 1H). **^{13}C NMR**(101 MHz, Chloroform-d) δ [ppm] 143.13, 129.93, 127.38, 125.85, 124.39, 113.32. GC-MS (EI): *m/z* = 110.1 [M^+], and theoretical value for C_6H_6S is 110.0.

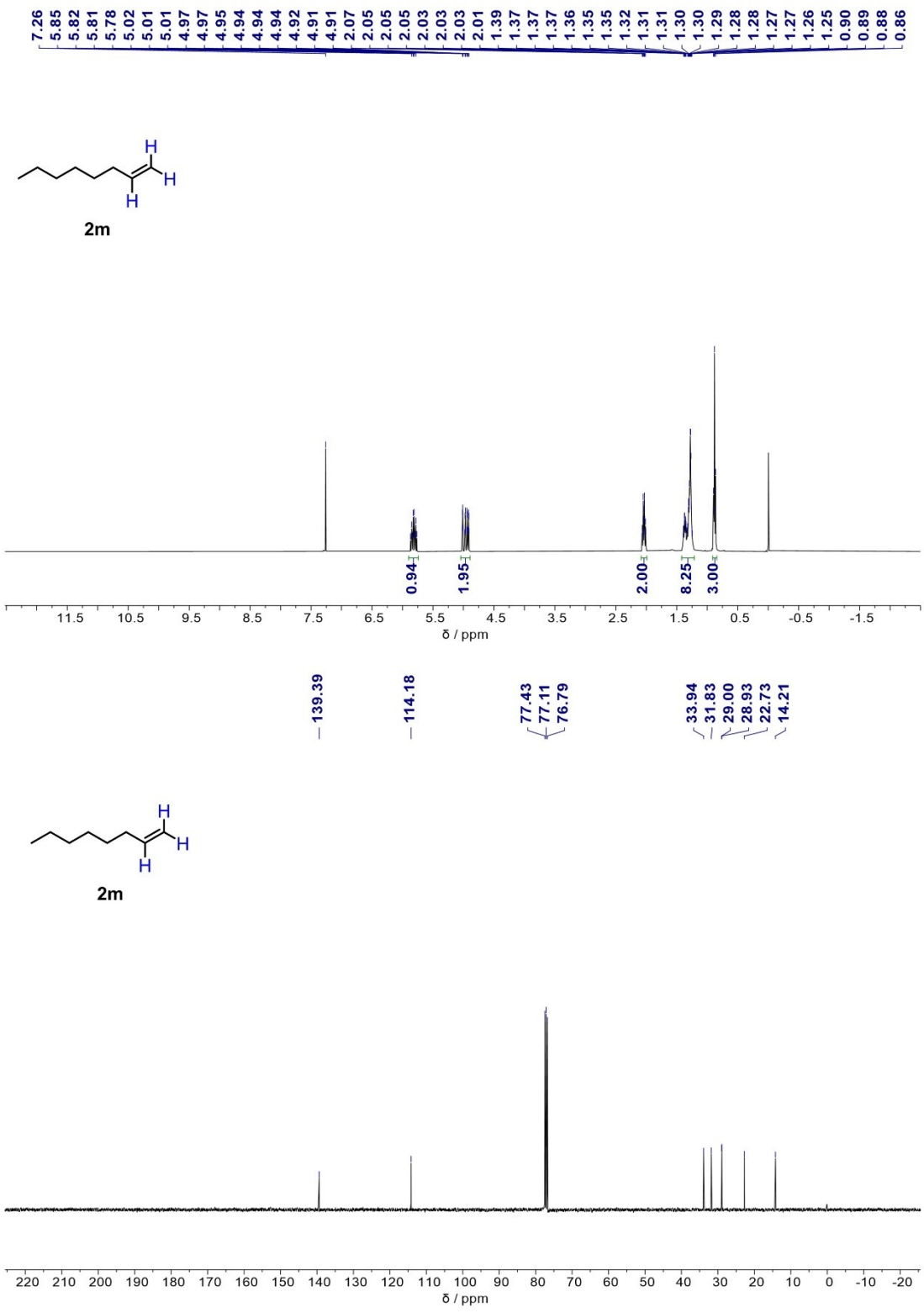

Fig. S44. **^{1}H NMR** (400 MHz, Chloroform-d) δ [ppm] 5.89–5.74 (m, 1H), 5.04–4.89 (m, 2H), 2.08–1.99 (m, 2H), 1.42–1.21 (m, 8H), 0.91–0.84 (m, 3H). **^{13}C NMR**(101 MHz, Chloroform-d) δ [ppm] 139.39,114.18, 33.94, 31.83, 29.00, 28.93, 22.73, 14.21. GC-MS (EI): *m/z* = 112.10 [M^{+}], and theoretical value for C_8H_{16} is 112.13.

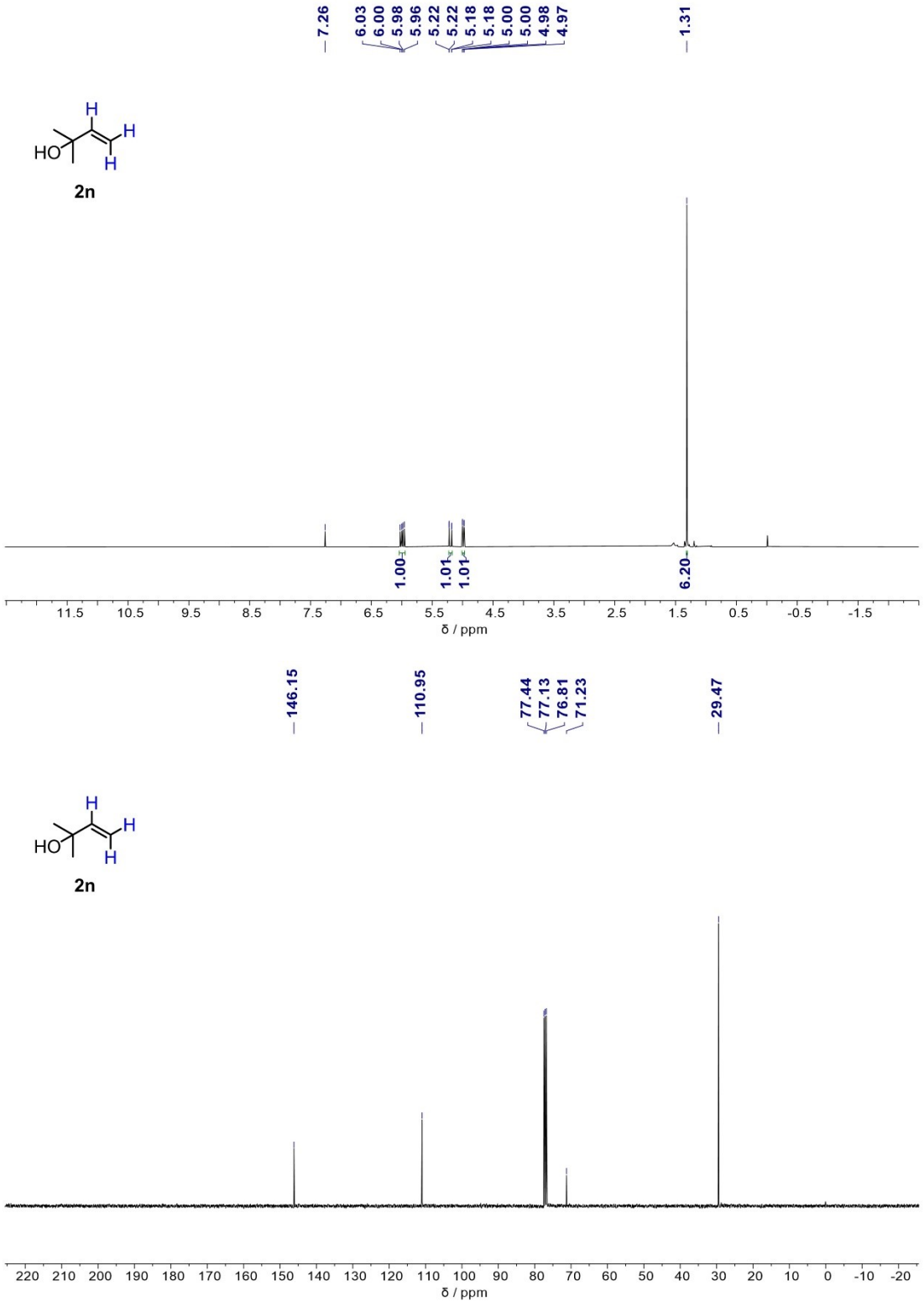

Fig. S45. **^{1}H NMR** (400 MHz, Chloroform-d) δ [ppm] 5.99 (dd, *J* = 17.2, 10.8 Hz, 1H), 5.20 (dd, *J* = 17.2, 1.2 Hz, 1H), 4.99 (dd, *J* = 10.8, 1.2 Hz, 1H), 1.31 (s, 6H). **^{13}C NMR**(101 MHz, Chloroform-d) δ [ppm] 146.15, 110.95, 71.23, 29.47. GC-MS (EI): *m/z* = 86.05 [M^{+}], and theoretical value for $C_5H_{10}O$ is 86.07.

Section 5. References

[1] P. X. Lei, S. Q. Liu, Q. R. Wen, J. Y. Wu, S. Wu, X. Wei, R. Feng, X. Z. Fu and J. L. Luo, Angew. Chem. Int. Ed., 2025, 64, e202415726.

[2] Z. Zhang, Z. Zhang, J. He, R. Wang, M. Yu, R. Zhang, X. Chen, Z. Shi and S. Feng, Angew. Chem. Int. Ed., 2025, 64, e202515485.